The Thesis Committee for Jayaram Athreya Hariharan

Certifies that this is the approved version of the following thesis:

Quantifying the Influence of Surface Processes on Subsurface Geometry in Deltaic Environments

APPROVED BY

SUPERVISING COMMITTEE:

Paola Passalacqua, Supervisor

David Mohrig

Quantifying the Influence of Surface Processes on Subsurface Geometry in Deltaic Environments

by

Jayaram Athreya Hariharan

Thesis

Presented to the Faculty of the Graduate School of

The University of Texas at Austin

in Partial Fulfillment

of the Requirements

for the Degree of

MASTER OF SCIENCE IN ENGINEERING

The University of Texas at Austin

May 2019

Acknowledgments

I would like to thank my advisor Dr. Paola Passalacqua without whom this work would not have been possible. She is truly an inspiration. Discussions with other faculty such as Dr. David Mohrig, Dr. Wonsuck Kim, Dr. Holly Michael, and Dr. Chris Paola have also helped me tremendously. The Environmental and Water Resources Engineering department has provided me with a wealth of support and encouragement from my peers. I would be remiss if I did not also thank the present and former members of the Passalacqua Research Group. This work would not have been possible without the prior efforts of Dr. Man Liang and Mr. Cory Van Dyk. Over the past two years, conversations with Kyle Wright, Isha Deo, Mariela Perignon, and Alicia Sendrowski have proven to be especially helpful and illuminating.

I would like to acknowledge the funding support making this work possible. This material is based upon work supported by the National Science Foundation Grant No. EAR-1719670.

Quantifying the Influence of Surface Processes on Subsurface Geometry in Deltaic Environments

Jayaram Athreya Hariharan, M.S.E.

The University of Texas at Austin, 2019

Supervisor: Paola Passalacqua

River deltas are densely populated and dynamically changing environments located at the boundary between land and sea. Population demands for water as well as rising sea levels are increasingly threatening aquifer water quality in deltaic regions. The rate at which aquifer contamination by salt water or other contaminants occurs is dictated, in part, by the arrangement of sediment within the subsurface. In this work, we examine the heterogeneity of the subsurface from a structural vantage to better understand how surface processes and geometry are linked to subsurface architecture. The numerical model, DeltaRCM, is applied to simulate delta evolution under a variety of input conditions. The resulting model outputs simulate 800 years during which the growing delta generates a subsurface volume that is over 40m deep. Surface channel properties and behavior, such as channel depths and channel planform decay rates are measured. Similarly, the structure of the sand bodies in the subsurface domain is evaluated. These different types of analyses, surface and subsurface, are ultimately compared to take a first-look at how channel properties in a deltaic environment may relate to subsurface structure and form.

Broadly, expectations about channel trends and subsurface structure from the field of geomorphology are supported. Channel depths decrease with distance from the

inlet, and as the input sand proportion increases. Similarly, the channelized fraction of the delta surface increases with higher input sand fraction values. In the subsurface, different types of channel behavior on the surface correspond to different structures. The sand bodies are larger when the surface channels are shallower and more mobile. In addition, the spatial continuity within strike sections (sections taken perpendicular to the inlet channel) increases with channel depth.

Comparisons of the modeled subsurface with stochastically re-arranged replicates have confirmed the assertion that surface processes create unique subsurface structures. When the input proportion of sediment contains at least 40% sand by volume, the average size of the subsurface sand bodies follows a power-law relation with respect to surface channel depths and the average channelized fraction of the delta platform. The range of spatial entropy (disorder) also increases with channel depth. Within models, with increasing distance from the inlet both channel depths and spatial entropy ranges decrease. Changing the input sediment proportions over the course of the delta evolution provides mixed results. Some channel parameters like channel depth are indistinguishable from steady input cases, while others are influenced by the initial topographic setup. In the subsurface, variable sediment input proportions create vastly different sand body geometries depending on the rate of variation of the input sand proportion. When the input sand proportion is gradually increased, the average sand body size becomes very large; however when the sand input is abruptly increased, the mean sand body value is less than a steady sand input analog.

Keywords: DeltaRCM; River Delta; Geomorphology; Channel Properties; Subsurface Characterization

Table of Contents

List of Tables

List of Figures

Chapter 1: Introduction

1.1 Significance and Motivation

Globally, about half a billion people live within or near river deltas (Syvitski et al., 2009). The population density in deltaic regions is more than seven times the global mean (Rahman et al., 2019). Coastal deltaic regions face both human induced stresses related to population growth and demands on resources, as well as stresses induced by climatic variability (Moser, Jeffress Williams, & Boesch, 2012). The study of river delta morphology and evolution is primarily motivated by an overarching goal of better understanding the processes under which river deltas form and change, in order to constrain predictions about the future of our world's deltaic systems. This work focuses on the *subsurface structure* beneath the surface of these river deltas.

"Why does the subsurface matter?" one might ask. The key motivation behind this investigation into the subsurface structure of delta stratigraphy is that the geometry of the subsurface is linked to the ability of pollutants and sea water to contaminate drinking water aquifers beneath the delta. Groundwater modeling has shown that the arrangement and heterogeneity of geologic facies within the subsurface greatly influences the distribution of breakthrough times for aquifer contamination (Khan et al., 2016). Our ability to constrain subsurface form is limited by few direct observations. Even in hydrocarbon applications, despite the economic incentive to accurately characterize a reservoir, typically only one-

trillionth of the subsurface is directly sampled (M. J. Pyrcz, Gringarten, Frykman, & Deutsch, 2006). As a result, we model and simulate subsurface geometries to try and approximate the properties and features of actual geology.

Broadly, we hypothesize that the surface channel features and geometries are related to the distribution and partitioning of sediment in the subsurface that develops. A set of different model realizations is generated to test the correlation between surface features and subsurface architecture; specific hypotheses to do so are outlined below.

1.2 Hypotheses

The following hypotheses are tested:

(A) Stratigraphy generated by DeltaRCM is different from stochastically arranged ('shuffled') stratigraphy with the same bulk parameters (e.g. facies proportions).

(B) Surface channel properties act as a first order control on the size and arrangement of sand lenses or sand bodies that are preserved in the stratigraphy.

  (i) Channel depth controls sand body thickness (in vertical direction)

  (ii) Channel mobility is correlated to sand body size

  (iii) Surface channel properties are reflected in the stratigraphy

(C) Changes in input sediment proportions produce deltaic stratigraphy that differs from the equivalent steady input case.

Chapter 2: Literature Review

This work is at the intersection of a few different areas of research, namely: numerical modeling, coastal geomorphology, and stratigraphic interpretation or subsurface characterization. Several different modeling strategies exist for simulating river deltas; for this analysis an informed decision was made to choose an appropriate model to work with in order to address the hypotheses. Techniques from remote sensing and geomorphologic analysis of surface processes of field, experimental and numerical deltas were evaluated and applied to characterize the surface behavior of the model. From stratigraphy and geostatistics, methods of analysis were considered to best characterize and understand the subsurface structures being generated by the numerical modeling.

2.1 Numerical Modeling of Deltas

There are several different ideologies when it comes to modeling physical systems. Complete physical modeling of hydrodynamics and sediment transport can be achieved, and numerical modeling programs such as Delft3D (Deltares, 2016) offer several different methods of solving these systems of equations. Other models spatially average features to estimate average delta dynamics, focusing on global features without modeling individual channels (Kim, Mohrig, Twilley, Paola, & Parker, 2009). In between these two extremes (complete physical modeling and bulk average modeling), exist a set of models known as reduced-complexity models. These models often use simplified physics to model individual channel features, but

avoid solving the computationally expensive equations associated with fluid dynamics. Several of these models exist to describe delta behavior (Liang, Voller, & Paola, 2015; Overeem, Syvitski, & Hutton, 2005; Seybold, Andrade, & Herrmann, 2007); for this investigation, DeltaRCM (Liang, Voller, & Paola, 2015) was chosen to model the formation of river deltas under different external conditions.

DeltaRCM is a reduced-complexity model that was built to simulate river delta formation (Liang, Geleynse, Edmonds, & Passalacqua, 2015; Liang, Voller, & Paola, 2015). DeltaRCM simulates river delta formation by routing water and sediment from an inlet channel through a domain using a weighted random walk. Physical rules govern the weighting of the water and sediment routing process. Natural variability is simulated by the random walk stochasticity which is weighted by physical weights, and is not deterministic. In DeltaRCM, two sediment types are input into the system, a small (mud) and large (sand) grained sediment. Sediment transport for each sediment type is governed by physical properties associated with the sediment grain size.

Numerical experiments have been conducted with DeltaRCM to ensure that the empirical rules governing the water and sediment routing produce results similar to other models, experiments, and field deltas (Liang, Geleynse, et al., 2015; Liang, Voller, & Paola, 2015). Additional studies have been conducted to evaluate the influences of subsidence on morphology using DeltaRCM (Liang, Kim, & Passalacqua, 2016). Similarly, the simulated deltas modeled with DeltaRCM have been used to construct a suite of metrics to evaluate the patterns and dynamics of the systems (Liang, Van Dyk, & Passalacqua, 2016).

2.2 River Delta Geomorphology

The concentration of our global population by these sources of agricultural and commercial activity is one reason why these river delta systems need to be better studied. Delta geomorphology is a broad field that encompasses the many different methods by which river deltas take shape and evolve. The prototypical way of evaluating river delta shape and properties is through the use of what is known as the Galloway Triangle (Galloway, 1975). The Galloway delta classification system places river deltas into 3 broad classes based on their 'dominant' morphological driver; river discharge, wave energy, or tidal energy. The types of deltas modeled in this study are fluvial-dominated deltas and are characterized in the Galloway Triangle framework as having elongate to lobate geometry with straight to sinuous distributary channels.

2.3 Delta Surface Characterization

Surface processes and characteristics are studied and quantified for field, experimental and numerically modeled deltas. Methods for identifying and analyzing fluvial features from satellite imagery have been developed (Isikdogan, Bovik, & Passalacqua, 2017; Schwenk, Khandelwal, Fratkin, Kumar, & Foufoula-Georgiou, 2017). Data from flume experiments has been taken and analyzed to characterize deltaic planform dynamics (Wickert et al., 2013). Numerical models have been applied to test the response and growth of deltas under various external conditions (Liang, Kim, & Passalacqua, 2016). While it is easier to measure and collect data from a numerical model than from satellites or experiments, many of the methods developed for those datasets are equally applicable to modeled deltas.

2.4 Stratigraphy and Stratigraphic Preservation

The modern geologic school of thought views stratigraphy as the end result of sedimentation and erosion processes (Barrell, 1917). Work by Wheeler furthered these ideas of space-time preservation of deposition events as a nonuniform and uneven process; in doing so, he also created the popular 'Wheeler Diagram,' format for describing time-stratigraphy graphically (Wheeler, 1958, 1964). More recently, a significant body of research is emerging that is related to the use of stratigraphy as a proxy record for the past (Trampush, Hajek, Straub, & Chamberlin, 2017), estimating the completeness of the stratigraphic record (Sadler & Strauss, 1990), and quantification of the 'shredding' of environmental signals by sediment transport processes (Jerolmack & Paola, 2010). All of this is to say that the processes governing both the development of stratigraphy and its preservation in the ultimate rock record are not precisely understood at this time.

2.5 Subsurface Modeling and Characterization

Quantitative description and characterization of spatial systems is the primary aim of geostatistics (Olea, 2009). From limited direct observations, geostatisticians and geologists work together to predict geologic formations and patterns. Challenges related to the computational cost of full 3-D modeling, limitations in data availability, or restrictions related to the geologic interpretations can result in hybrid or combined workflows for developing geologic models (Jørgensen, Høyer, Sandersen, He, & Foged, 2015). Broadly, the different types of subsurface models are process-based models, object-based models, training image based models, and variogram based models (Linde, Renard, Mukerji, & Caers, 2015). DeltaRCM, as a forward

process-based model, captures and preserves some of the surface dynamics in the subsurface stratigraphy. While not a pure geologic model, DeltaRCM produces a geologic formation based prior surface processes, analogous to a process-based geologic model, but with the advantage of capturing the surface dynamics responsible for the geology.

Chapter 3: Methods

3.1 Model Runs

54 total model runs were conducted using DeltaRCM to simulate approximately 800 years of delta evolution (Table 3.1 & Table 3.2). Model conditions such as the grid cell resolution, sea level rise rate, and volumetric fluxes of water and sediment into the system were kept constant for all of the model runs (Table 3.1, for a full list of model parameters see Appendix A). The input sediment concentration was varied between the different model runs, and for some of the model runs, the input sediment concentration was allowed to vary during the simulation. Due to the stochastic components of DeltaRCM, namely the weighted random walk, multiple model replicates were conducted for each simulated condition (Table 3.2). The primary focus of this investigation was the constant sediment input proportions, and as a result more model replicates were created. The variable input sediment cases represent preliminary work at investigating the impact of a changing input sediment concentration on delta morphology and subsurface expression.

Table 3.1: Summary of Model Constants

Model Constants

Parameter	Value
Simulation Duration	800 years
Cell Dimensions (X × Y × Z)	50m x 50m x 5cm
Initial Sea Level Elevation	0m
Relative Sea Level Rise	60 mm/year
Inlet Channel Width	250 m
Inlet Water Flux	1250 m^3/s
Inlet Sediment Flux	1.25 m^3/s
Basin Depth	5 m

Table 3.2: List of All Modeled Scenarios

Modeled Scenarios

Constant Input Sediment Concentrations	Number of Realizations
20% Sand, 80% Mud	8
30% Sand, 70% Mud	8
40% Sand, 60% Mud	8
50% Sand, 50% Mud	8
60% Sand, 40% Mud	8
70% Sand, 30% Mud	8
Varying Input Sediment Concentrations	**Number of Realizations**
20% → 70% Sand, 80% → 30% Mud (varies gradually)	3
20% → 70% Sand, 80% → 30% Mud (varies abruptly)	3

Typical delta platforms developed as semi-circular areas radiating from the inlet channel (Figures 3.1, 3.2 and 3.3). Section views taken perpendicular to the inlet direction (strike sections) provide a clear look at how the different input sediment proportions can generate different stratigraphy (Figures 3.1, 3.2 and 3.3). The variation of input sand proportions during a simulation was conducted in two ways: for one set of realizations the variation in sediment proportion was abrupt, and a mud-dominated input instantly became sand-dominated, for the other set of realizations the transition from mud to sand-dominated input was gradual (Figures 3.3 & 3.4).

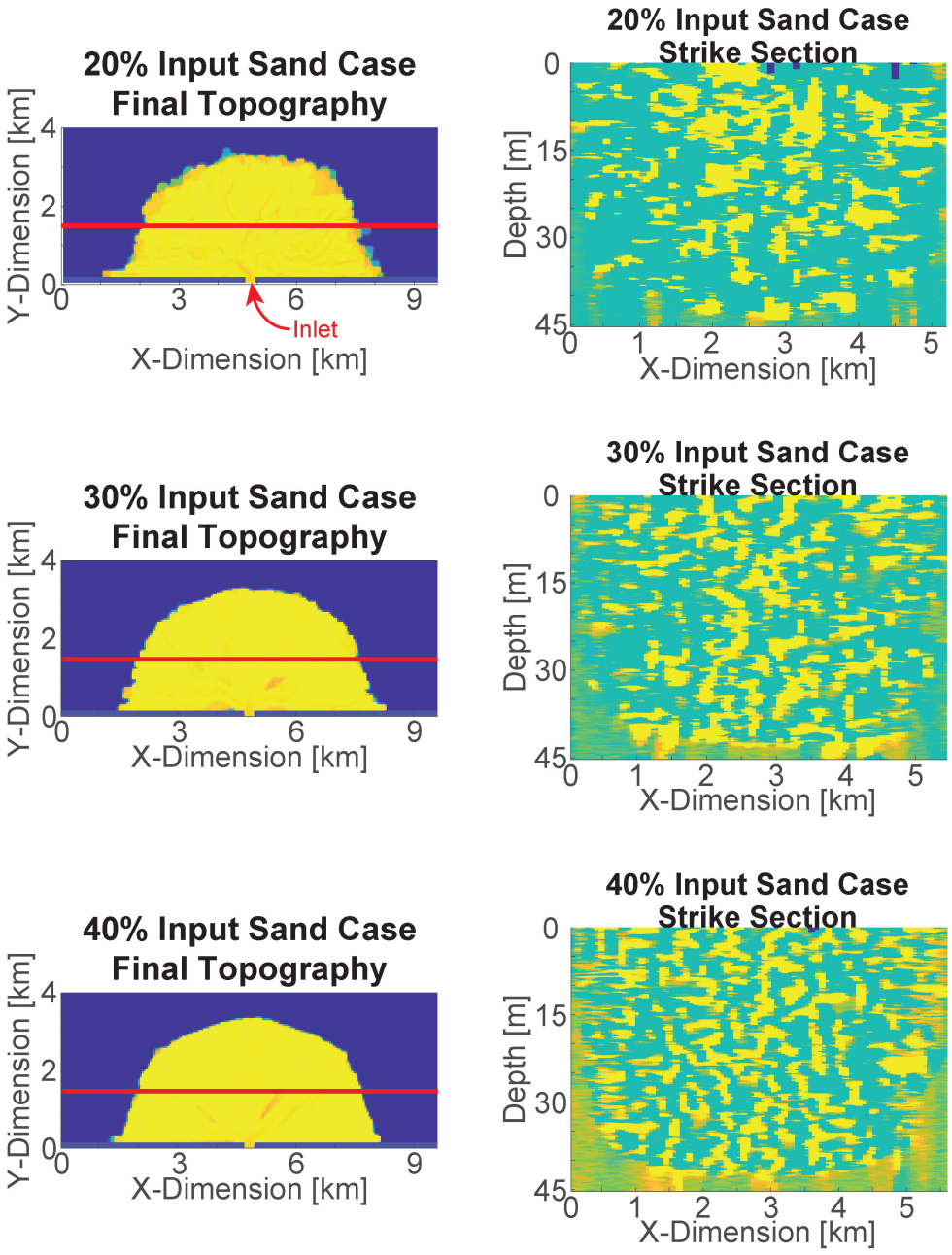

Figure 3.1: Final model topographies with associated strike sections taken 1.5km from the inlet

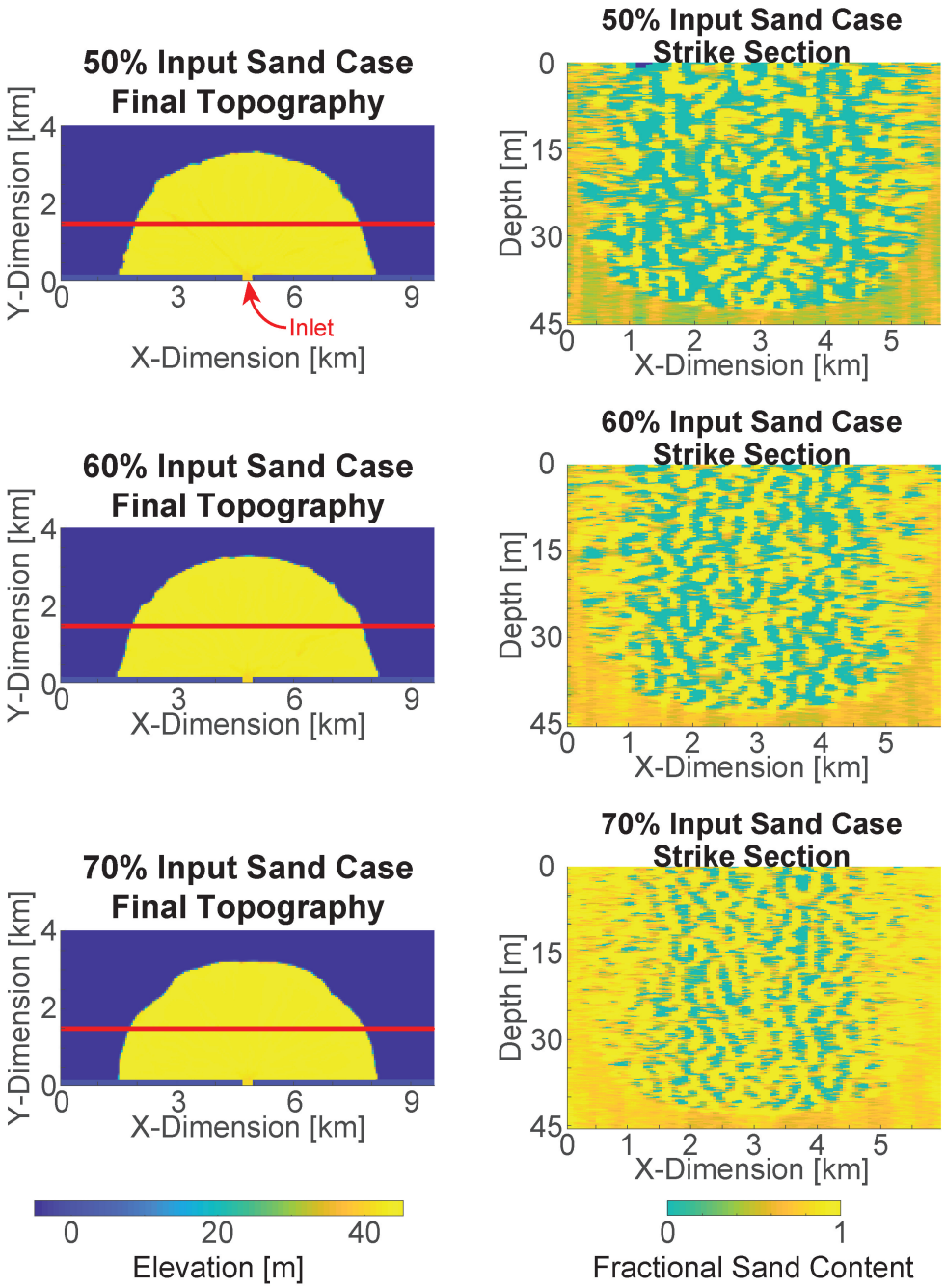

Figure 3.2: Final model topographies with associated strike sections taken 1.5km from the inlet

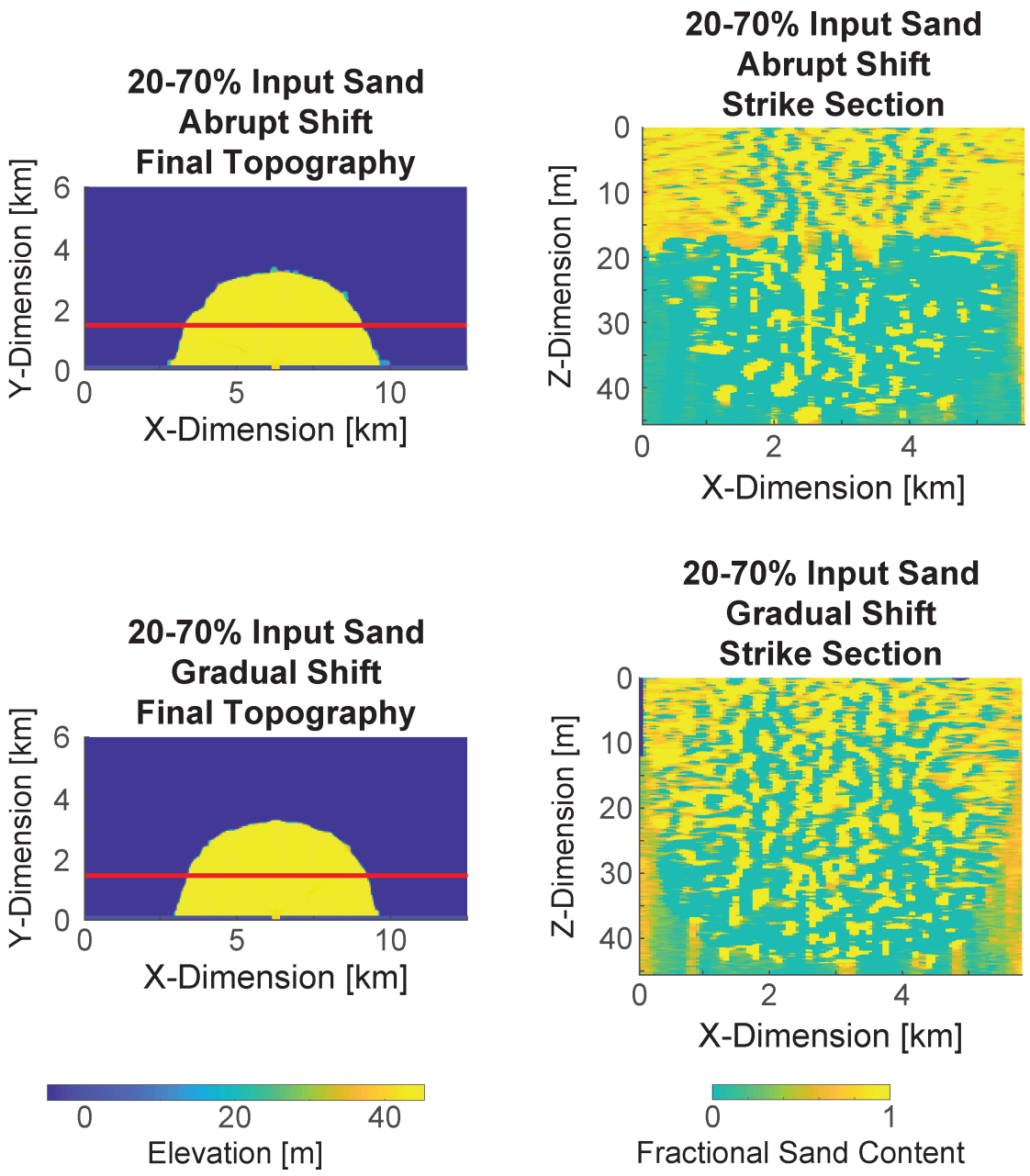

Figure 3.3: Final model topographies for the variable input sediment cases, with associated strike sections taken 1.5km from the inlet

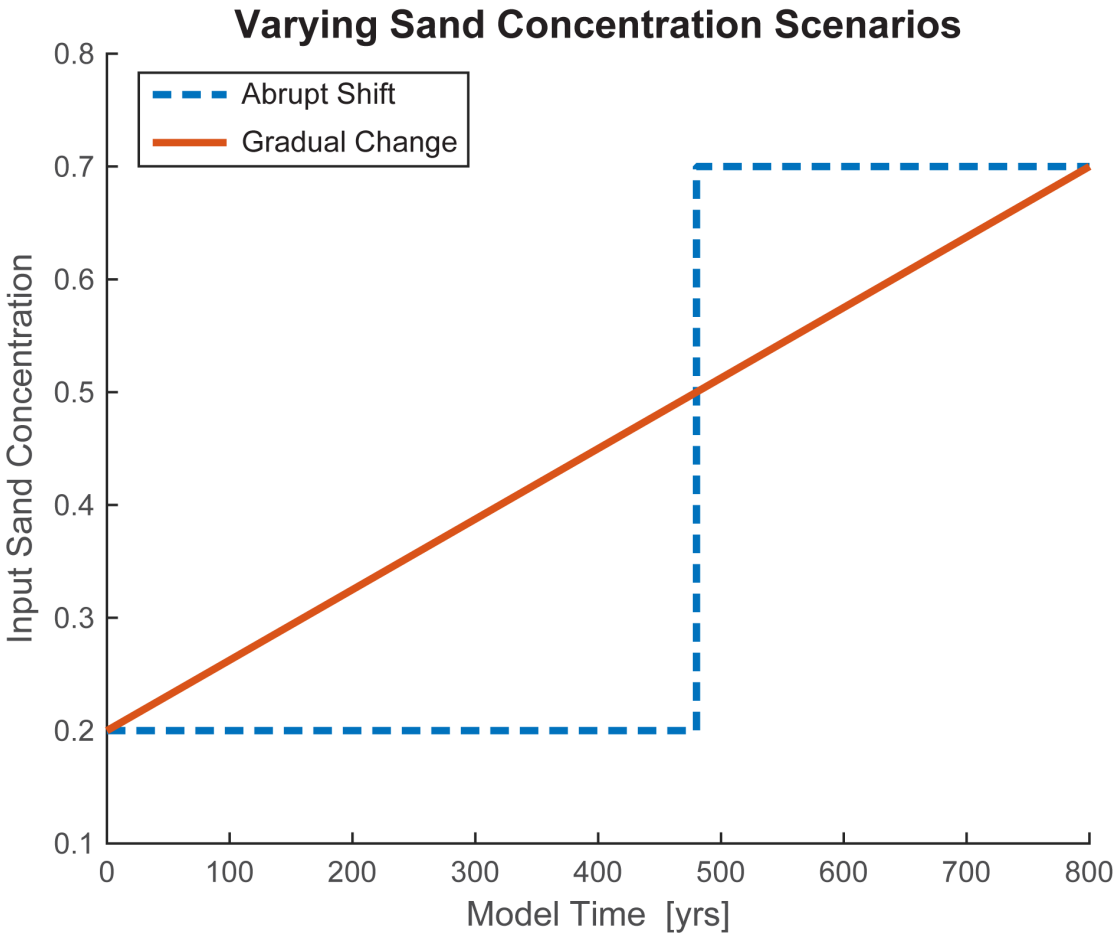

Figure 3.4: Time series of the input sand proportion to the models for the variable sediment proportion scenarios

3.2 Developing Synthetic Stratigraphy

To test the dependence of the subsurface structure on the surface dynamics, the stratigraphy generated by the model is manipulated to generate 'synthetic' stratigraphies.

3.2.1 'Shuffled' Stratigraphy

Stochastic re-arrangement, or 'shuffling,' of the modeled stratigraphy was performed. The following steps were taken to 'shuffle' the modeled stratigraphy:

1. Final model stratigraphy is identified
2. Vertical 'chunk' size or the depth of block to be collected and stacked is chosen
3. The final stratigraphy is randomly searched and vertical blocks (of the 'chunk' size) are pulled and stacked together
4. This newly assembled 'shuffled' stratigraphy is then trimmed to be the same size as the original modeled stratigraphy

Several different 'chunk' sizes were used to generate a set of synthetic stratigraphy which preserved different amounts of the original model structure. An illustration is provided to depict the shuffling process graphically (Figure 3.5). Varying this vertical resolution of the shuffling is one method of changing the degree of preservation of the initial stratigraphic structure developed by the mode (Figure 3.6).

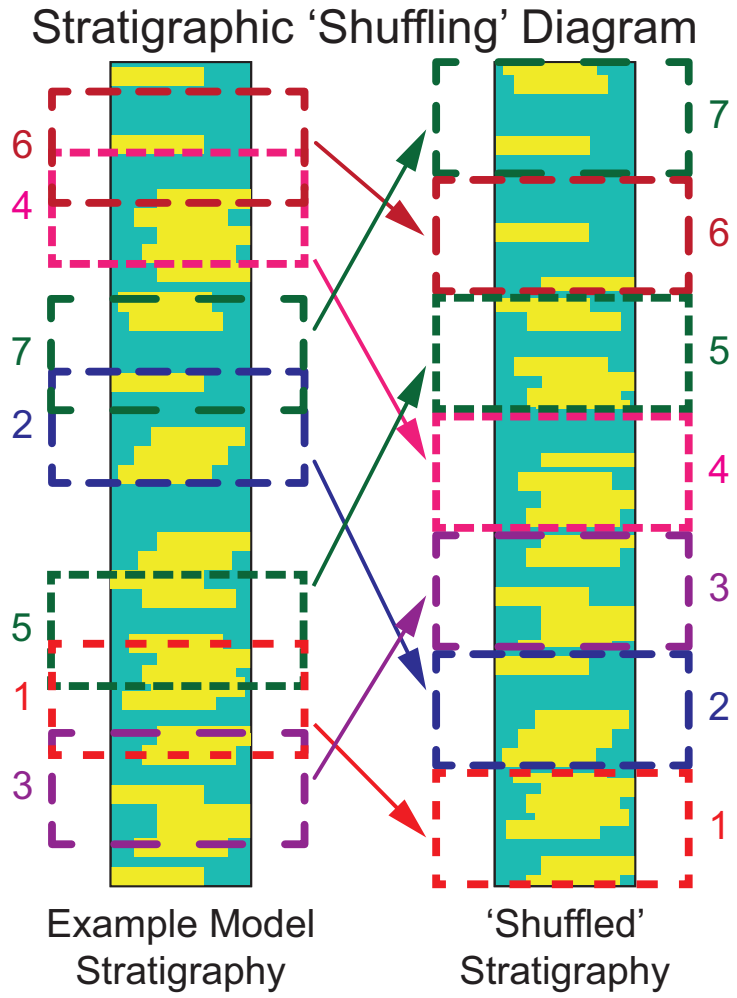

Figure 3.5: Example of stratigraphic ‘shuffling’ workflow

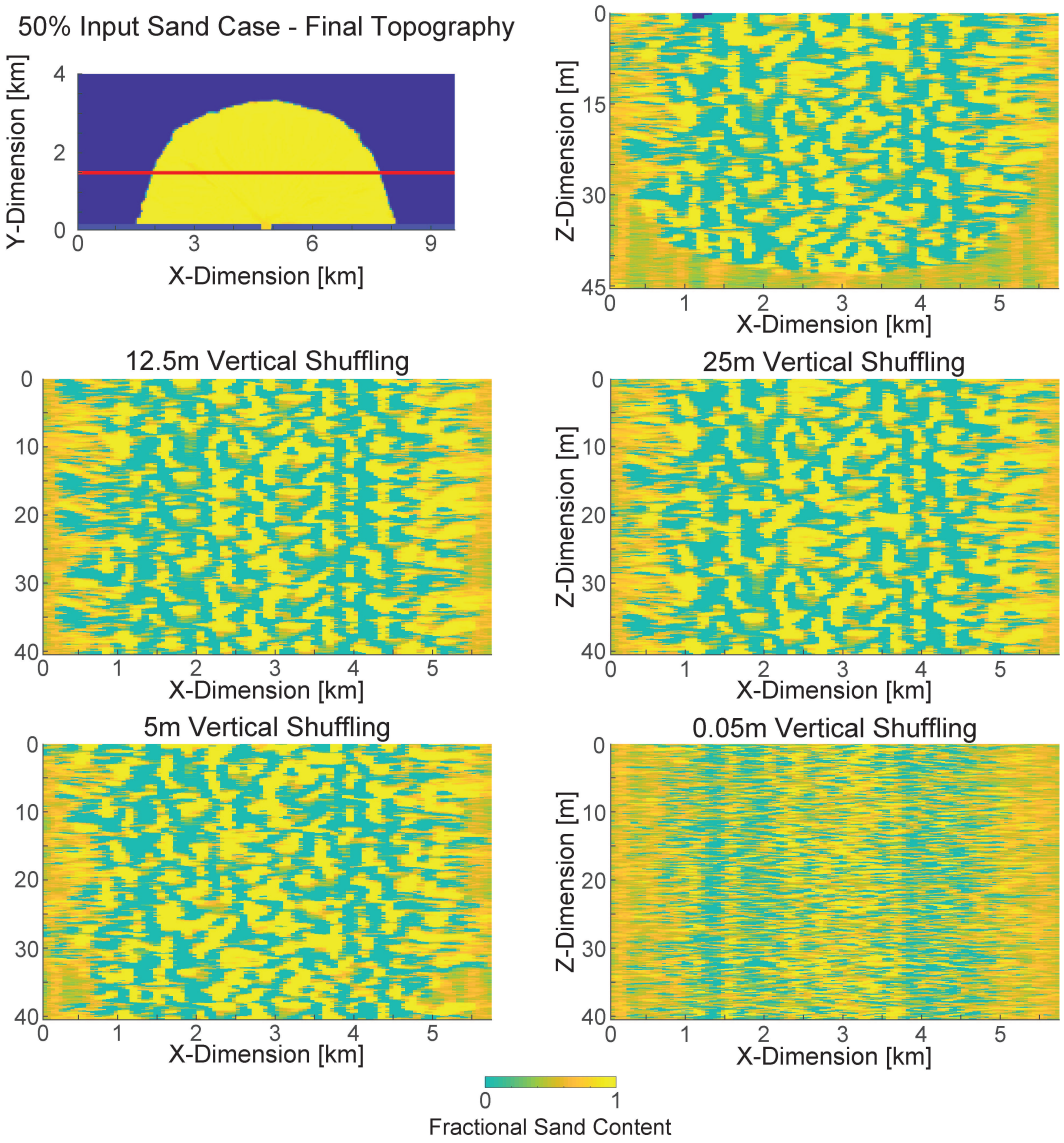

Figure 3.6: Examples of shuffled strike sections from the 50% input sand case

3.3 Channel Map Extraction

Surface channel locations are identified as a binary channel map by selecting cells with flow velocities above a threshold of 0.3 m/s (the model velocity threshold for suspended sediment transport) as described in Liang, Van Dyk, and Passalacqua

(2016). These binary channel maps are then used to quantify channel properties and mobility. Using the channel map, further information can be extracted from the model such as channel depth information (Figure 3.7).

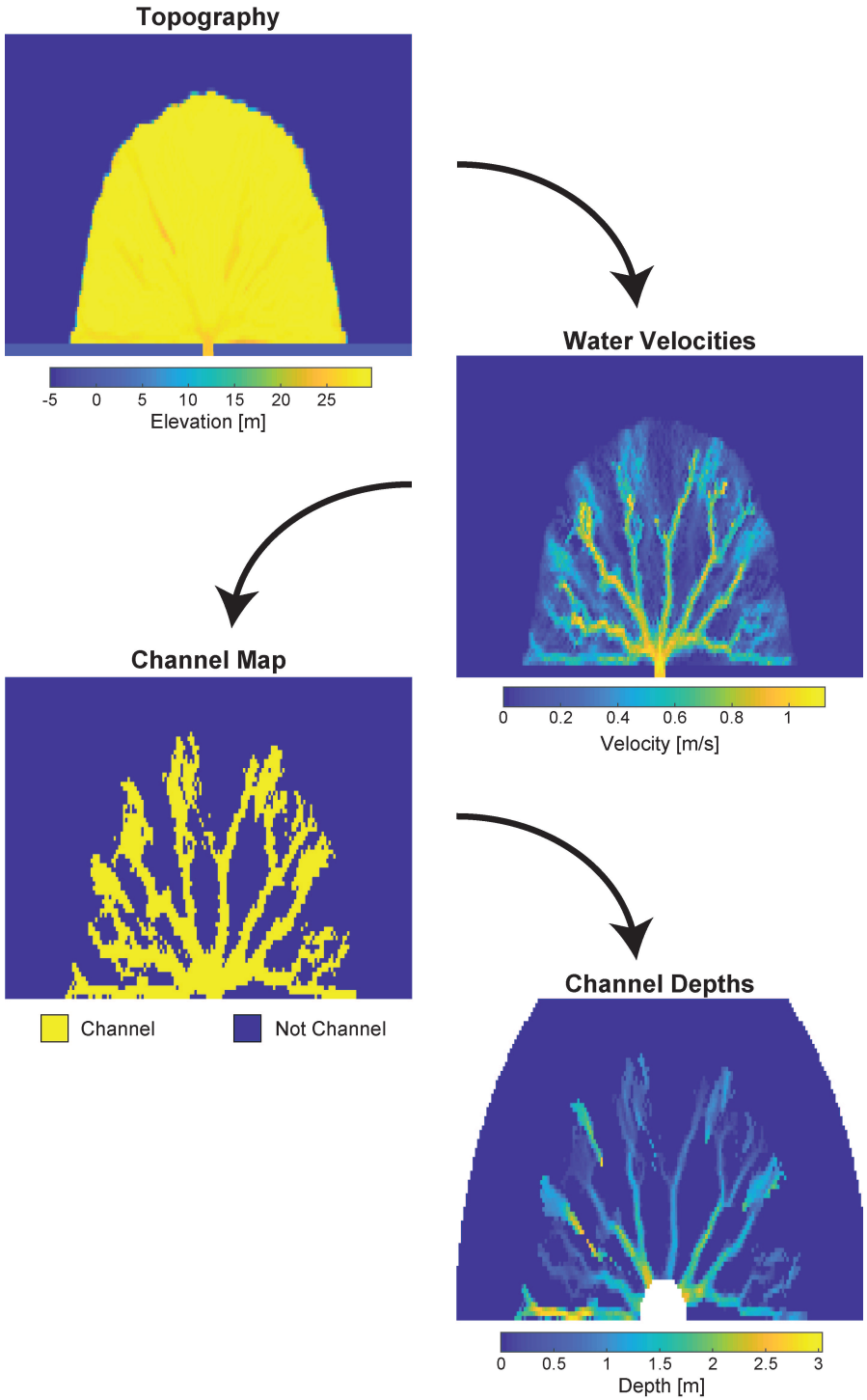

Figure 3.7: Example of channel map and then channel depth data extraction from a 50% input sand case model realization

3.3.1 Surface Channel Fraction

The fractional amount of channelized pixels relative to the entire delta platform is computed over the model run duration. The channel map is used to obtain the number of pixels at for each output, and the overall land area is computed using the landmap process described in Dyk (2015) and Liang, Van Dyk, and Passalacqua (2016). The equation outlining the computation of the channel fraction at a given time t, is provided in Equation 3.1.

$$\text{Channel Fraction}\,(t) = \frac{\text{Channelized Pixels}\,(t)}{\text{Total Land Pixels}\,(t)} \tag{3.1}$$

3.3.2 Surface Channel Mobility

Surface channel mobility is quantified using the extracted channel maps. From the channel maps, the channel planform decay metric is used to characterize channel mobility per Cazanacli, Paola, and Parker (2002); Liang, Kim, and Passalacqua (2016).

The channel planform decay metric measures channel mobility by measuring the duration over which channelized pixels remain channelized. A sliding window approach is taken to measure this channelization decay over a 40 year window. This method is analogous to the method described in Liang, Kim, and Passalacqua (2016) which was conducted over a 33 year time window.

After the data for the channel decay metric has been collected, a exponential decay equation is fit to the data (Equation 3.2). By using an exponential decay equation,

the rate of channel planform decay can be quantified, and is represented by the parameter b in Equation 3.2.

$$\text{Channel Decay} = ae^{-b(\text{Time Lag})} + c \tag{3.2}$$

3.4 Subsurface Characterization

3.4.1 Autocorrelation

The autocorrelation function is typically used to characterize the timescale for 'memory' within a timeseries, or the length of time over which a signal value influences subsequent data values. Autocorrelation is a measure of self-similarity, and therefore is the comparison of a signal with itself at a time lag. When evaluating the subsurface, we use depth in the stratigraphy as an analog for time, and apply this autocorrelation methodology to sediment cores and sections.

$$\text{ACF}_k = \frac{\text{COV}\left(x_t, x_{t+k}\right)}{\sigma_x^2} \tag{3.3}$$

Equation 3.3 presents the standard autocorrelation function for a variable x at lag k where COV indicates the covariance function and σ is the standard deviation. When computing the autocorrelation for a section of the stratigraphy, the average autocorrelation is computed in the direction of interest.

Autocorrelation curves begin at 1, as the covariance of x_t and x_t is equal to the variance. From there, the autocorrelation function declines because the correlation between a lagged signal is very rarely as correlated as the signal at zero-lag. The rate of decay in the autocorrelation function is approximated by fitting a line to

the first few points. The slope of this fit line provides an estimation of the initial rate of decay in the autocorrelation function, or the rate at which the signal loses correlation with itself.

3.4.2 'Geobody' Analysis

The characterization of so-called 'geobodies' in a subsurface field involves the discretization of individual cells as either permeable or non-permeable (Hovadik & Larue, 2007). This discretization of the field can be set by a permeability threshold defined by a desired flow capacity, or it can be determined via an assessment of the distribution of a subsurface property of interest. For example, if the permeability distribution of a field is highly bi-modal, it would be appropriate to choose a geobody threshold value between the two modes. In DeltaRCM, the subsurface variable recorded is a percentage of sand content per cell; the rest of the material is mud. Sand has a larger grain size than mud, and is the more permeable facies in the DeltaRCM simulations. From the distribution of sand content in the model stratigraphy cells (Figure 3.8), a threshold of 50% sand content was chosen for the geobody discretization. This decision was made because the sand content distributions were highly bimodal with the modes located at the end-members (fully mud cells and fully sand cells). The probability distribution functions (Figure 3.8) were obtained via kernel density estimation using a normal kernel (which is why the tails exceed practical values for fractional data).

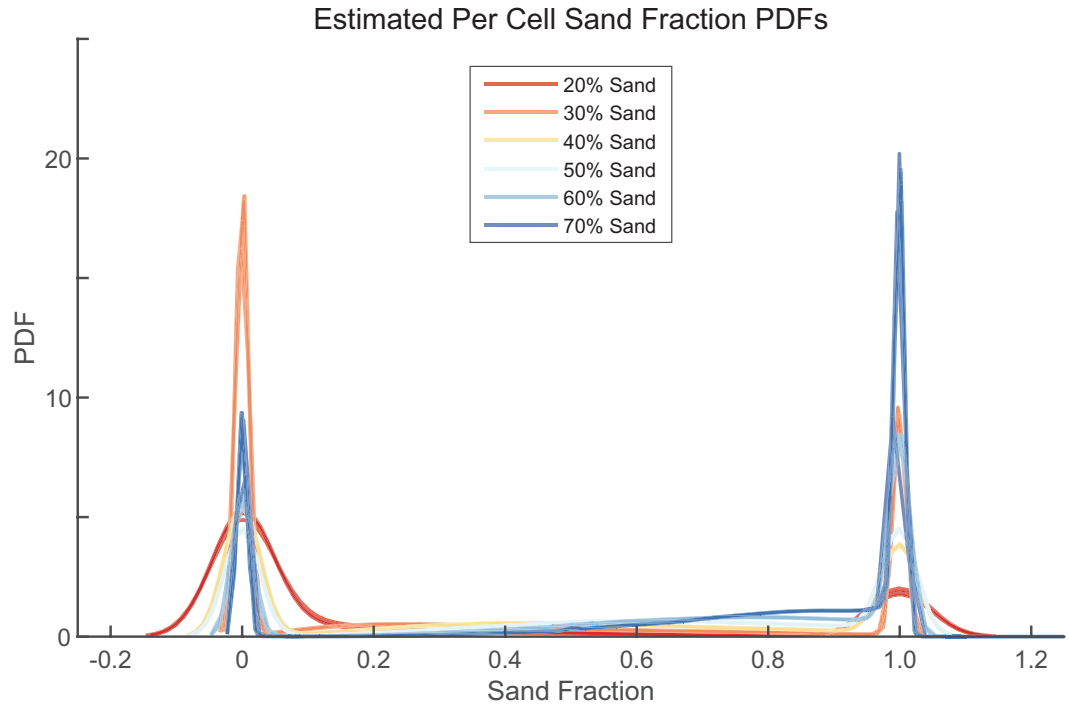

Figure 3.8: Kernel Density Estimated Sand Distribution in Model Cells

In the full 3-D model stratigraphy, the most prevalent geobodies are comprised of a single cell, skewing median values to the volume of a single cell. At the other end, while the right tail of the distribution is not particularly heavy, the large outliers are very far from the rest of the data. This results in mean values that are artificially skewed higher by the extreme values at the upper end of the distribution.

In the 2-D sections, the cross-sections of the geobodies are identified as well. Strike sections are used for this analysis; the shape, area, and perimeter of the sand lenses are obtained. These distributions are similarly skewed like the 3-D geobody distributions.

The delineation of geobodies is an application of connected component analysis.

This analysis has been performed in MATLAB utilizing the image processing toolbox (The Mathworks Inc., 2018).

3.4.3 Variogram Analysis

Variogram analysis is a common method in geostatistics used to determine the typical element size, or the spatial continuity, within a region of interest (Matheron, 1963). The generalized computation of the isotropic (semi) variogram is shown in Equation 3.4 where N is the number of pairs, and $Z(x_i)$ and $Z(x_{i'})$ are the measurements of variable Z at locations x_i and $x_{i'}$.

$$\gamma(h) = \frac{1}{2N_j} \sum_{i,i' \in N_j}^{N_j} \left[Z(x_i) - Z(x_{i'}) \right]^2 \tag{3.4}$$

The variogram is applied in 1-dimension to study the spatial scales of vertical continuity. The vertical variogram is computed across the strike sections taken, similar to the autocorrelation process. The average of the vertical variograms across the strike sections are used to evaluate the average vertical spatial continuity scale. The raw variograms are smoothed and averaged across the strike sections, and then the results across the model replicates are combined to develop ensemble average variogram results.

3.4.4 Entrogram Analysis

The entrogram is a geostatistical tool which is based on Shannon Entropy, the foundational element of Information Theory (Bianchi & Pedretti, 2018). Similar to the variogram, the entrogram is a methodology for quantifying spatial scales. In the Information Theory framework, these ranges translate to spatial scales of

disorder (entropy). Per Bianchi and Pedretti (2018), the definition of the isotropic entrogram is described in Equation 3.5. The 2-D entrogram is computed over the strike sections using a variably scaling window for the computation of the local geologic entropy due to the disparity in the number of cells in the X and Z directions (Figure 3.9).

$$H_R(I) = \frac{1}{n_s(I)} \sum_{i=1}^{n_s} H_{R,i}(I) \tag{3.5}$$

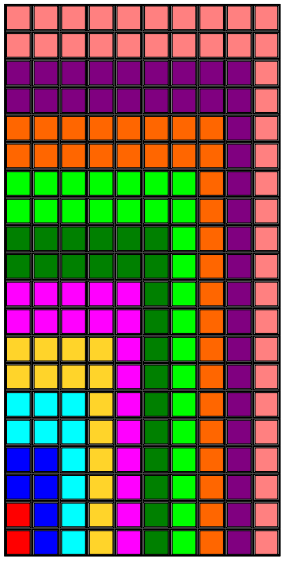

Figure 3.9: Schematic of uneven scaling of local entropy window - each color represents the expanded sliding window over which local geologic entropy is computed at different scales

Chapter 4: Results

4.1 Importance of Process-Based Modeling

In this section the results pertaining to Hypothesis (A) are presented. The difference between the synthetic stratigraphy generated via 'shuffling' is compared with the modeled stratigraphy which was process formed.

4.1.1 Changes to Autocorrelation Length

Between the different modeled scenarios, the vertical autocorrelation functions were different (Figure 4.1). The initial rate of decay in autocorrelation, from sections taken 1.5km from the inlet, increases as the input sand concentration increases from 20% sand to 70% sand.

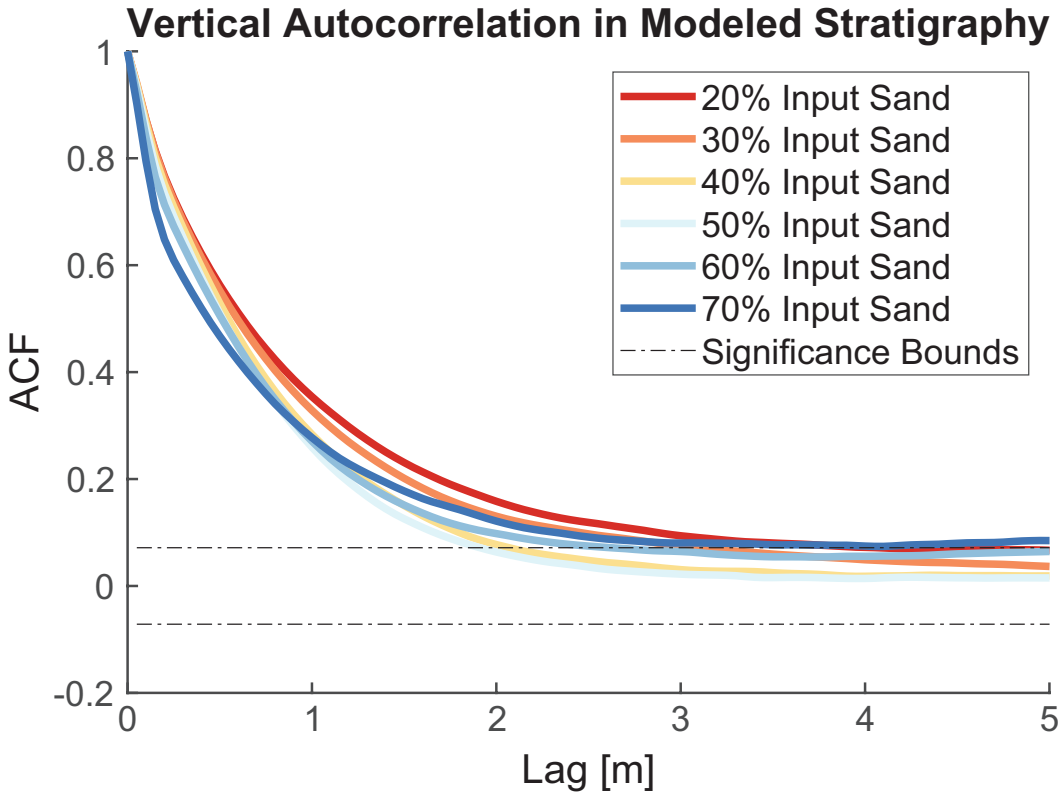

Figure 4.1: Average Vertical Autocorrelation for Strike Sections Taken at y=1.5km. Ensemble averaged results are depicted as solid lines. Horizontal dashed black lines represent the bounds of statistical significance for the autocorrelation results.

As the resolution of the shuffled blocks decreases, less physical structure is preserved, and the initial rate of decay of the autocorrelation function increases (Figures 4.2 & 4.3). First-order estimates for initial autocorrelation decay for the 20% input sand model case, and the shuffled scenarios derived from the 20% sand model are provided (Table 4.1). The trend observed between the model case and the different shuffling realizations is consistent between the different input sand scenarios, these additional figures are provided in Appendix E.

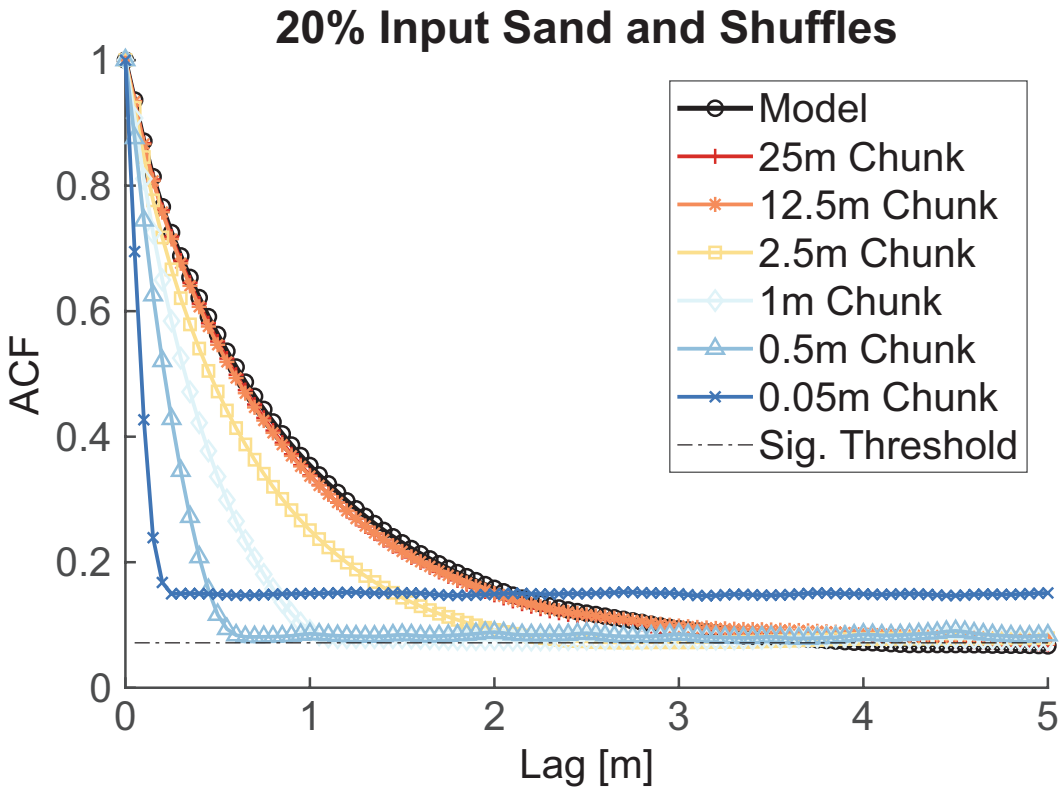

Figure 4.2: Averaged Vertical Autocorrelation for Modeled and Shuffled 20% Input Sand Strike Sections Taken at y=1.5km

Table 4.1: Vertical ACF - 20% Input Sand Case (Strike Section at Y = 1.5km)

First-Order ACF Decay Rates - 20% Sand Model and Shuffled Cases

Shuffling Resolution	Decay Rate [m^{-1}]
Model Case	−1.17
25m Shuffle Chunks	−1.20
12.5m Shuffle Chunks	−1.21
2.5m Shuffle Chunks	−1.41
1m Shuffle Chunks	−1.75
0.5m Shuffle Chunks	−2.40
0.05m Shuffle Chunks	−4.16

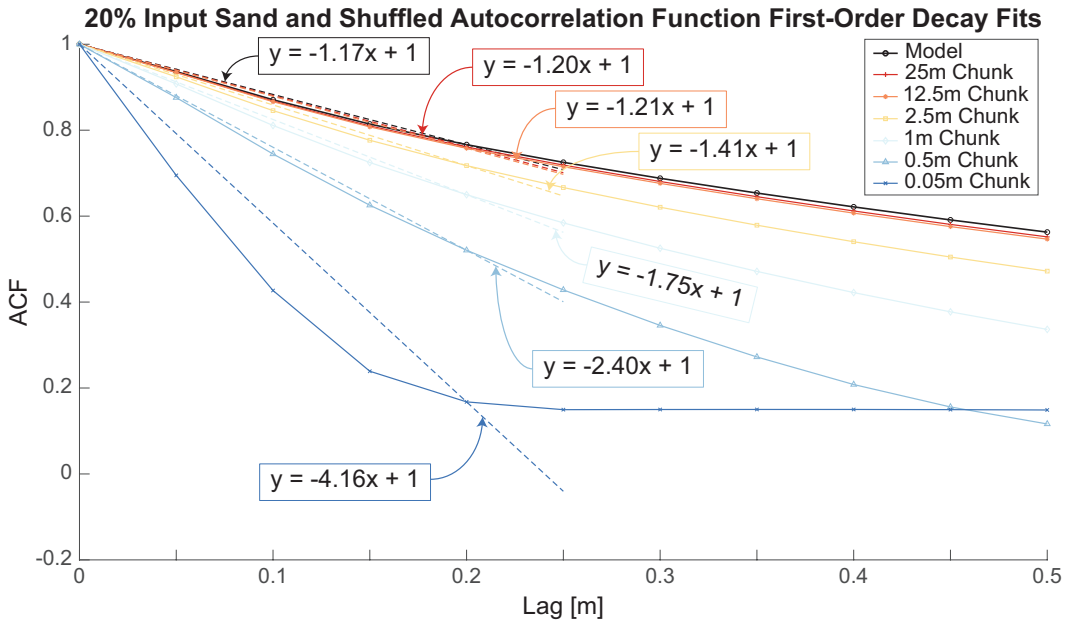

Figure 4.3: First-order fits to estimate the decay of the autocorrelation function for the 20% input sand model and shuffled realizations.

4.2 Surface Channel Characteristics

In this section, results and data related to the properties of surface channels in different model scenarios are presented.

4.2.1 Surface Channel Depths

The distributions of surface channel depths is skewed towards lower (<1m) depths. Boxplots and histograms (Figure 4.4) provide a visualization of the distribution of surface channel depths for each input sediment proportion condition; the data from all of the model runs and all of the modeled time has been aggregated and is included in the plots. Ensemble statistics suggest that both the mean and median channel depth values decrease as the proportion of sand input to the system is increased (Table 4.2).

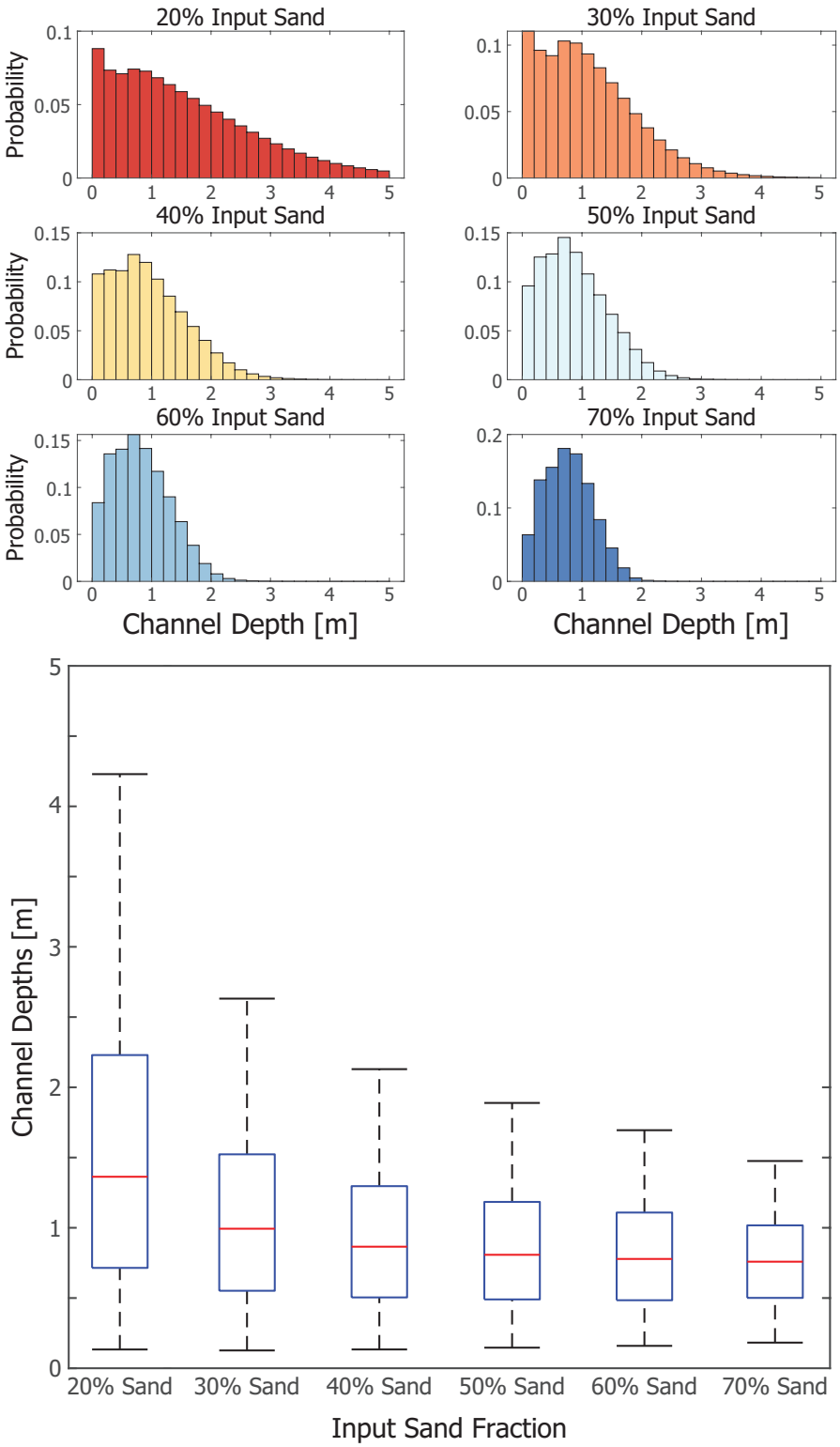

Figure 4.4: Channel Depth Distributions

Table 4.2: Ensemble Channel Depth Statistics - Aggregated across model time and all model runs

Channel Depth Statistics

Input Sand Concentration	Mean Channel Depth [m]	Median Channel Channel Depth [m]	Channel Depth Std. Deviation [m]
20% Sand	1.6738	1.3632	1.3905
30% Sand	1.1352	0.9934	0.8418
40% Sand	0.9617	0.8653	0.6356
50% Sand	0.8844	0.8077	0.5493
60% Sand	0.8318	0.7781	0.4825
70% Sand	0.7792	0.7586	0.3982

For the variable input sand conditions, the channel depth distribution and statistics are calculated before and after Year 480 (location of abrupt sand increase per Figure 3.4) as well as over the entire distribution (Table 4.3). The average input sand fraction for the two cases, the abrupt and gradual changes in input sand concentrations, are 40% and 45% sand respectively. The overall channel depth statistics for the gradual and abrupt varying input sand concentration cases have mean and median values which are similar to the 40% steady input sand case for the abrupt variation, and between the 40% and 50% steady input sand cases for the gradual variation.

Table 4.3: Ensemble Channel Depth Statistics - Variable Input Sand Conditions

Variable Sand Input - Channel Depth Statistics

Variable Input Sand Case	Time Frame [yrs]	Mean Channel Depth [m]	Median Channel Depth [m]	Channel Depth Std. Deviation [m]
Abrupt	0 - 480	1.2281	1.0762	0.9259
Abrupt	480 - 800	0.7949	0.7454	0.4512
Abrupt	0 - 800	0.9844	0.8417	0.7320
Gradual	0 - 480	0.9814	0.8793	0.6714
Gradual	480 - 800	0.8312	0.7604	0.5061
Gradual	0 - 800	0.9085	0.8133	0.6016

In addition to delta-wide collection and analysis of channel depth values, the channel depths along specific strike transects were also collected. The average channel depth values for strike transects at Y=1, 1.5, and 2 km decrease with distance from the inlet, and with increasing input sand fraction (Figure 4.5).

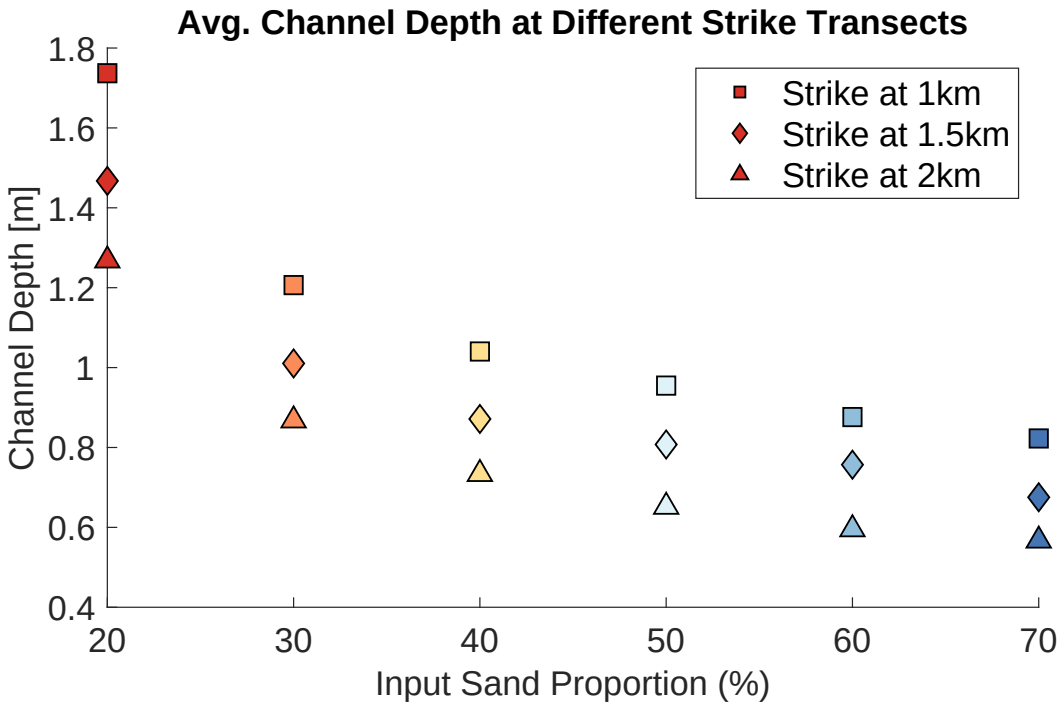

Figure 4.5: Average Channel Depths at Different Strike Transects

4.2.2 Surface Channel Fraction

The proportion of the surface of the delta that is occupied by channels over time is initially very high and declines as the channel platform grows, ultimately achieving a pseudo-steady state condition once the platform is fully developed (Figure 4.6). Ensemble mean values for the channel fraction as well as the ensemble standard deviations are determined for each modeled scenario. These channel fraction values are also temporally averaged for each model condition so a singular time-averaged channel fraction for each input sand condition can be obtained (Figure 4.7).

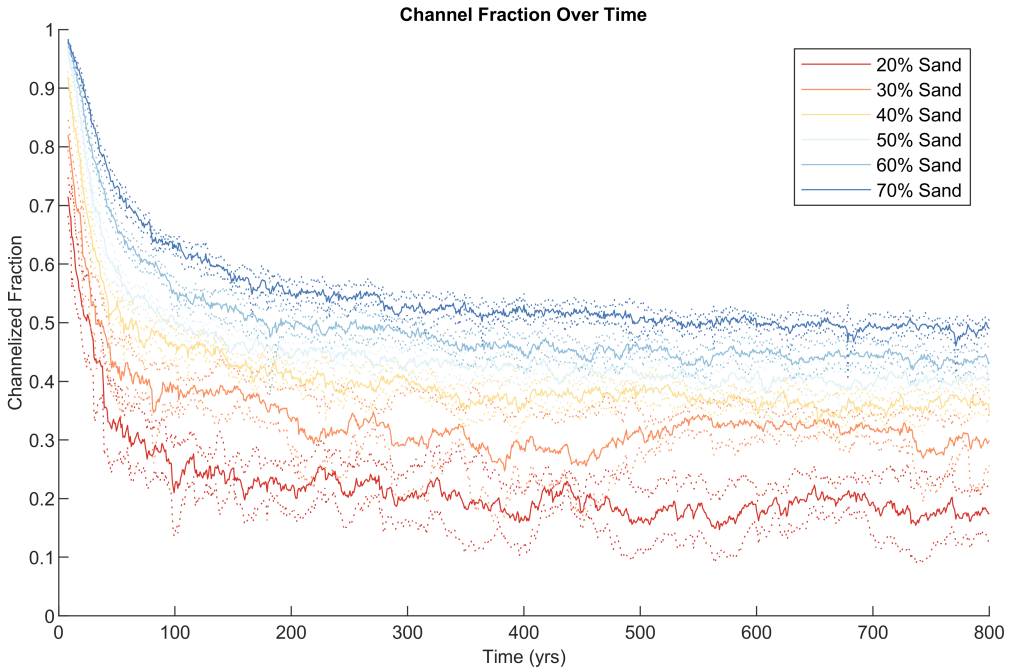

Figure 4.6: Ensemble averaged channel fraction over time. Solid lines represent ensemble mean values, dotted lines are ±1 standard deviation bounds.

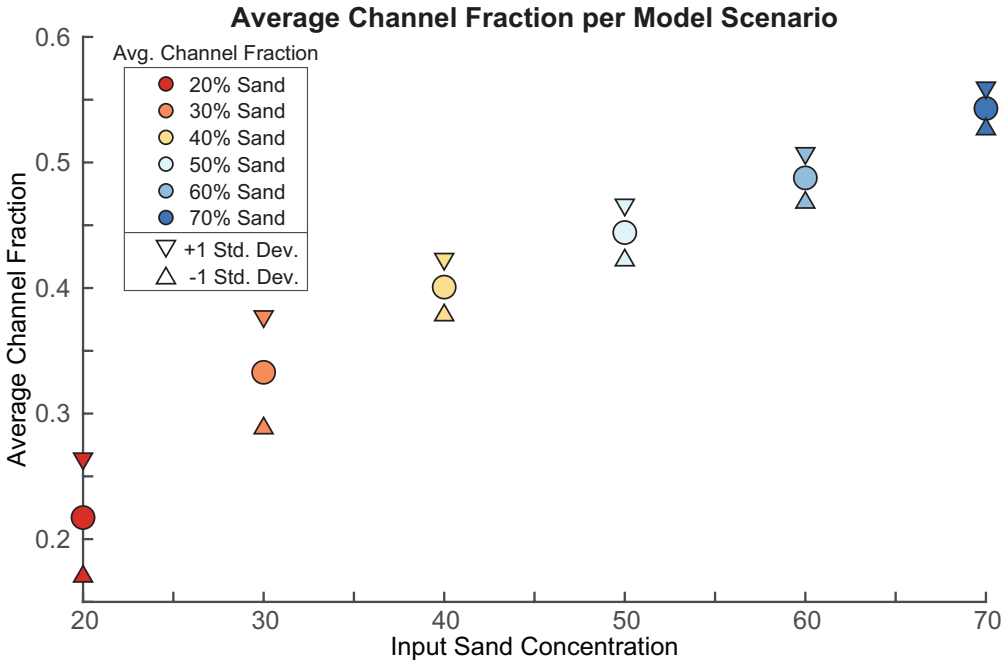

Figure 4.7: Temporally averaged channel fraction plotted against input sand proportion for the respective model scenario

For the variable input sand conditions, both the gradual and abrupt transition cases have channel fraction timeseries that initially resemble the 20% steady input sand case, however they change as their input sand concentrations are altered over the duration of the simulations (Figure 4.8). The variable sand input cases, although they have bulk sand concentrations of 40 and 45% ultimately, do not express channel fractions above the average channel fraction calculated for the steady 30% input sand scenarios.

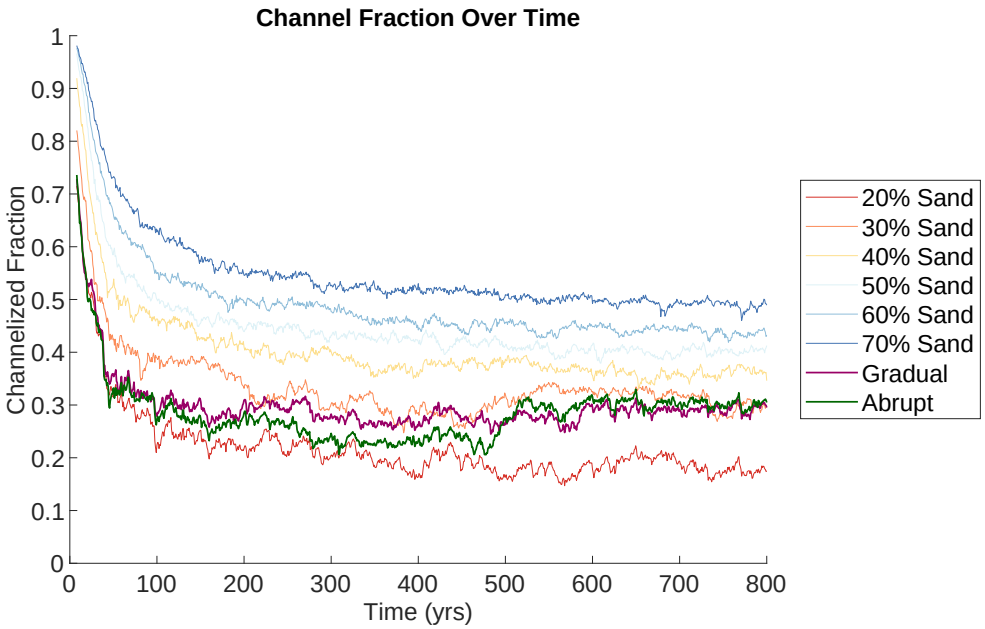

Figure 4.8: All channel fraction ensemble averages over time (standard deviation bounds omitted for clarity)

4.2.3 Surface Channel Mobility

The surface channel mobility is evaluated as described in Section 4.2.3 (Figure 4.9). The data is fit using an exponential decay equation of the form: $y = ae^{-bx} + c$, R^2 values all exceed 0.99, suggesting that this equation form is capable of representing this data accurately (Table 4.4).

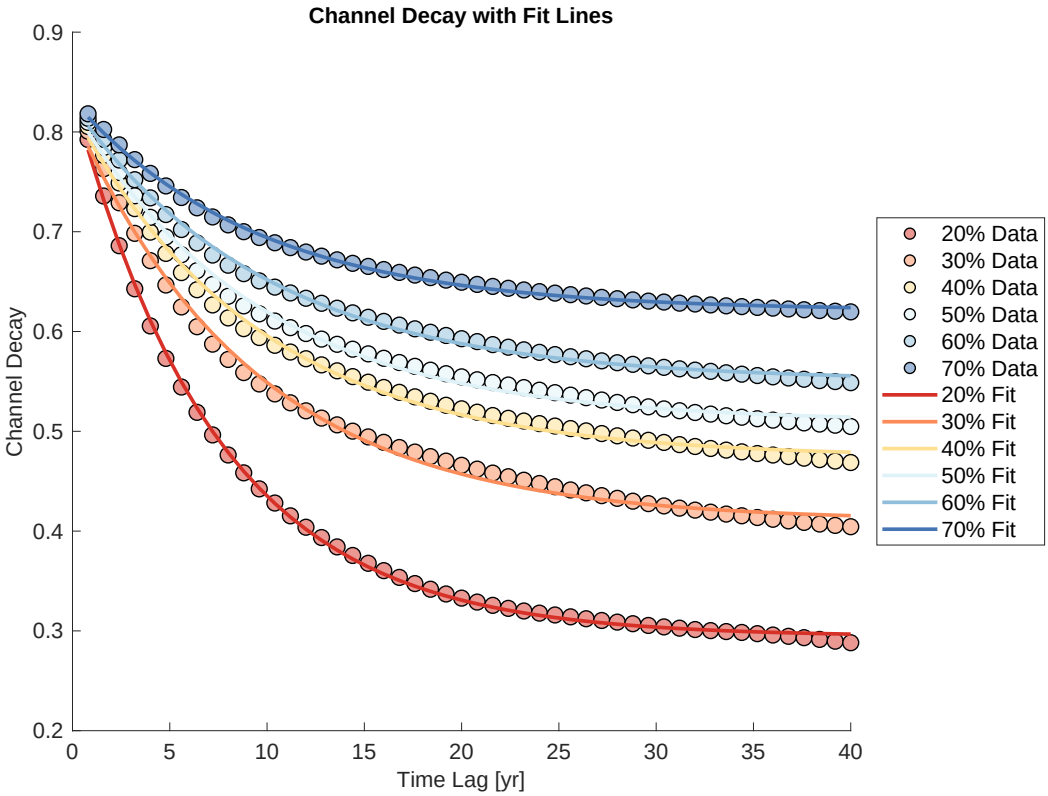

Figure 4.9: Channel decay data values plotted as circles; fit exponential decay equations plotted as solid lines.

Table 4.4: Exponential Decay Fits to Channel Decay Data

Channel Decay Exponential Fit Parameters

Input Sand Fraction	a	b	c	R^2
20% Sand	0.5434	0.1350	0.2943	0.9992
30% Sand	0.4094	0.1081	0.4100	0.9950
40% Sand	0.3485	0.1050	0.4738	0.9950
50% Sand	0.3158	0.1054	0.5096	0.9941
60% Sand	0.2766	0.1005	0.5507	0.9959
70% Sand	0.2110	0.1059	0.6209	0.9976

The variable input sand case channel decay was also computed and compared to the results from the steady input sediment cases. These results suggest that the variable input sediment cases had similar average channel dynamics, and the rate of channel planform decay was in between that of the steady 20% and 30% input sand scenarios (Figure 4.10).

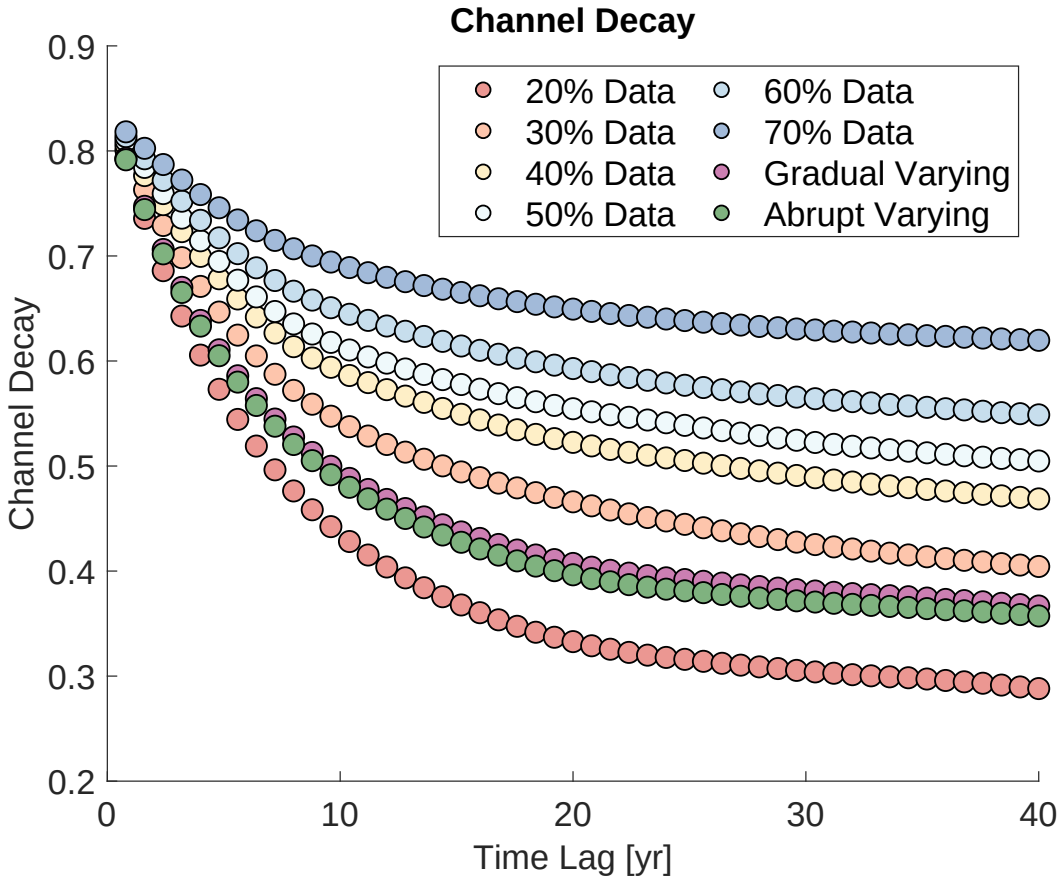

Figure 4.10: Channel decay data values for all scenarios.

4.3 Subsurface Structure

In this section, results and data related to the structure and characteristics of the subsurface structure developed in the models is presented.

4.3.1 Vertical Sand Package Sizes

Vertical sand packages in a given strike section of stratigraphy are determined by moving column by column across the section and counting the contiguous sand cells to measure sand bodies. After counting all of the vertical sand bodies present, they are averaged to get an idea of the vertical sand package size preserved in a given strike section, these average values tend to increase as the input sand supply does (Figure 4.11 & Table 4.5).

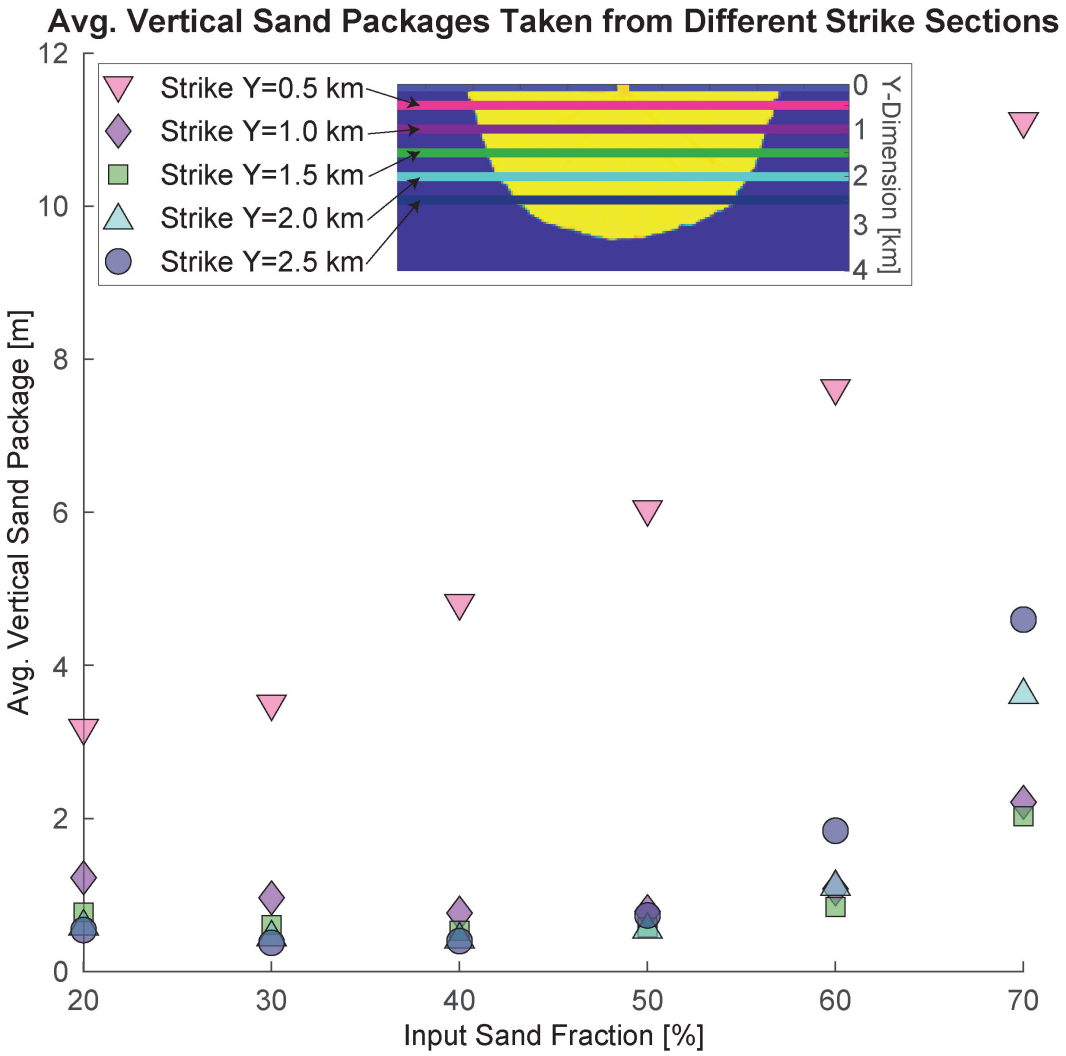

Figure 4.11: Average vertical sand package size for different sediment input proportions

Table 4.5: Average vertical sand package size at different strike sections

Average Vertical Sand Package Size

Input Sand Fraction	Y = 1 km	Y = 1.5 km	Y = 2 km
20% Sand	1.2245	0.7717	0.5875
30% Sand	0.9627	0.6088	0.4455
40% Sand	0.7633	0.5330	0.4185
50% Sand	0.7819	0.5774	0.5454
60% Sand	1.0791	0.8415	1.1049
70% Sand	2.2110	2.0269	3.6115
Gradual Case	0.9018	0.6413	0.5767
Abrupt Case	1.4622	1.0394	1.4417

4.3.2 Vertical Spatial Correlation (Variograms and Entrograms)

The variogram and entrogram are applied in 1-D to measure the ranges of spatial correlation in the vertical direction for strike sections taken 1.5km from the inlet. These metrics are computed in 1 dimension along the depth of the section, and averaged across the length of the section. Results suggest that the correlation ranges are not the same; the variogram range is much shorter than that of the entrogram (Figure 4.12 & Figure 4.13).

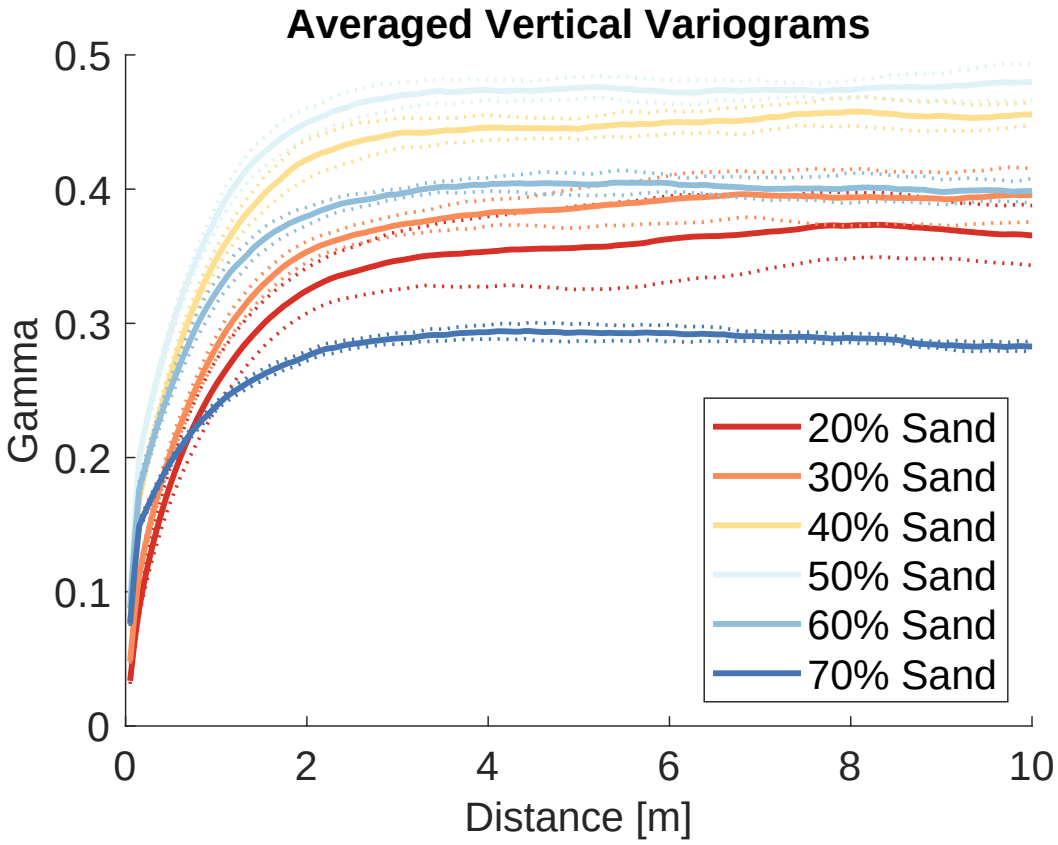

Figure 4.12: Averaged 1-D variograms taken in the vertical direction

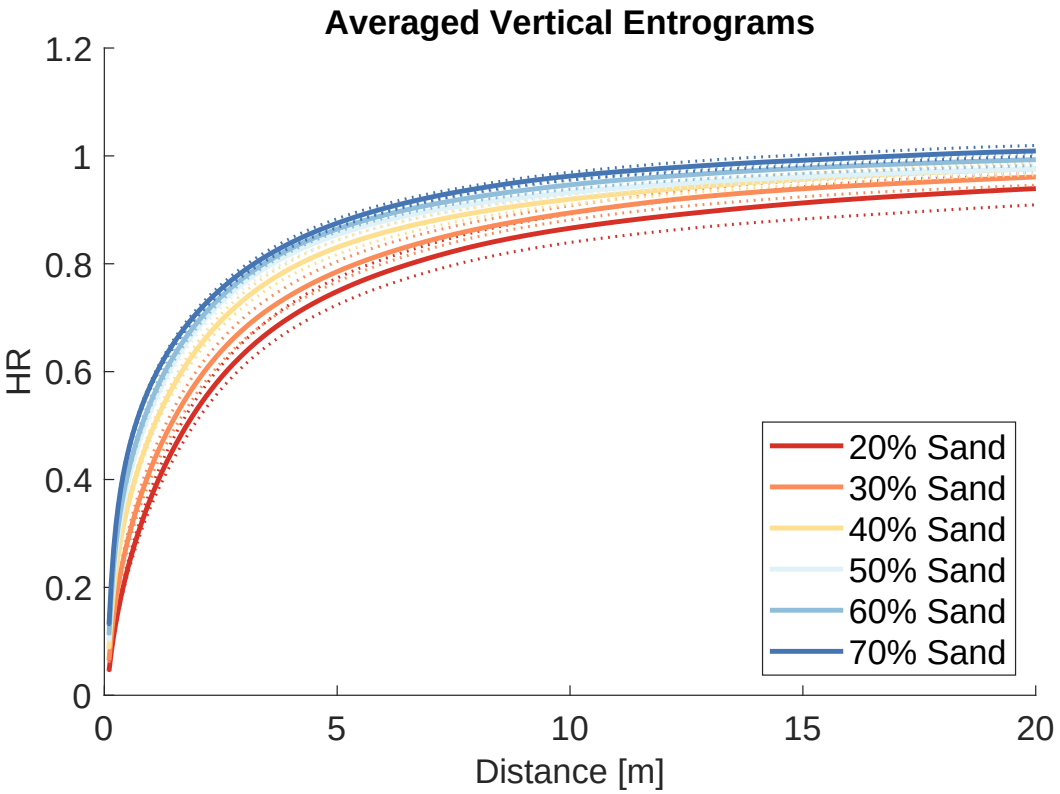

Figure 4.13: Averaged 1-D entrograms taken in the vertical direction

4.3.3 Strike Section 2-D Entrograms

For strike sections taken 1, 1.5, and 2 km from the inlet, 2-D isotropic entrograms have been computed to estimate the spatial ranges in the stratigraphy. The assumption of stationarity in the field is violated, and the local entropy at certain scales exceeds the global entropy resulting in entrogram values above 1 (Figure 4.14). Averaged ensemble spatial correlation ranges tend to decrease as the input sand fraction increases (Table 4.6).

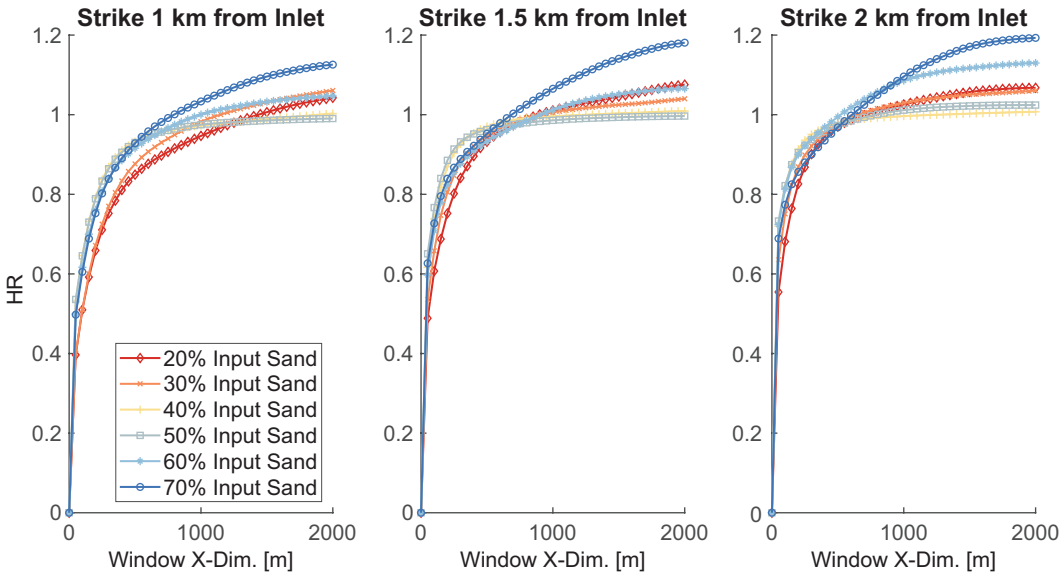

Figure 4.14: 2-D Entrograms for strike sections taken at different distances from the inlet

Table 4.6: 2-D Entrogram Average Range in X and Z directions (X [km], Z [m])

2-D Entrogram Average Range (X [km], Z [m])

Input Sand Fraction	Y = 1 km	Y = 1.5 km	Y = 2 km
20% Sand	1.4000	0.9188	0.9125
30% Sand	1.1438	0.9375	0.7188
40% Sand	1.5125	0.9188	0.9188
50% Sand	3.5438	1.2313	0.7125
60% Sand	1.0188	0.8750	0.5750
70% Sand	0.8188	0.7688	0.5688
Gradual	5.7167	5.0000	3.7833
Abrupt	5.6333	4.7167	4.4167

4.3.4 2-D Strike Section Geobody Data

2-D geobodies are calculated at strike sections taken 1, 1.5, and 2 km from the inlet. The ensemble average areas are presented on a semi-$\log_{10}$ axis because of the extremely high geobody areas found in the high sand fraction (60% and 70% input sand) model runs (Figure 4.15).

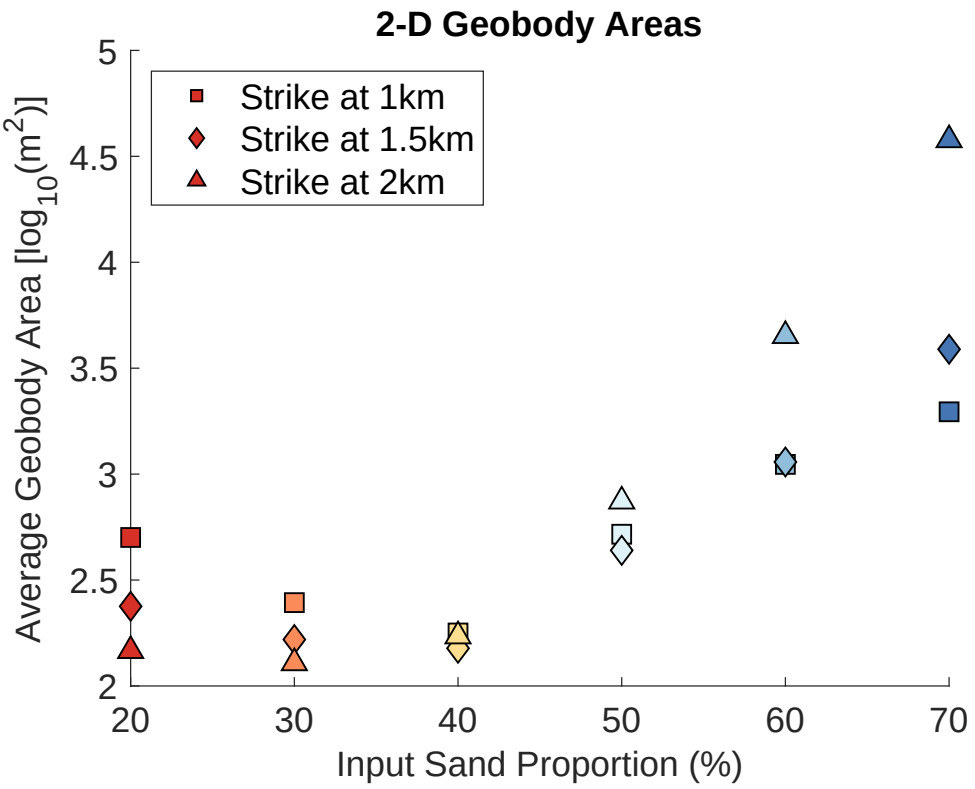

Figure 4.15: Ensemble Averaged 2-D Geobody Areas ($\log_{10}$)

4.3.5 3-D Geobody Volumes

The distribution of all geobody volumes identified in the modeled subsurface for the different model runs is highly skewed (Figure 4.16). The distributions were highly skewed towards small geobodies, prompting a log-transform of the data. Even

after log-transformation, the distributions remain highly skewed to the right. In the highly sandy scenarios, there are very high volumes for a few geobodies, these extreme values bias distribution descriptors such as the mean value. Typically, the median value can be used in place of the mean value when a distribution contains extreme outliers. However in the geobody volume distributions, there are so many small geobodies, that the median values are simply the smallest values.

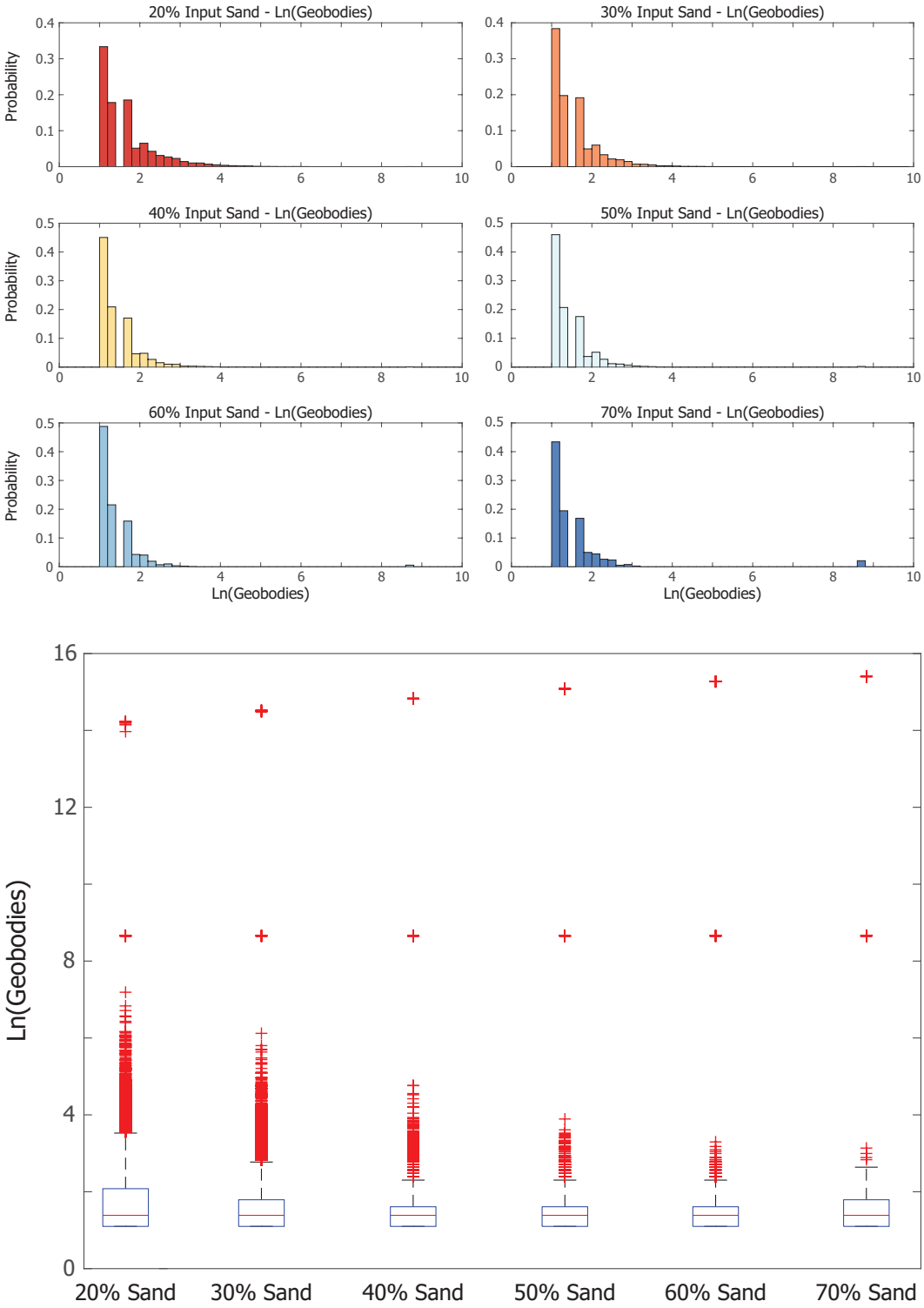

Figure 4.16: Natural Log Geobody Volume Distributions

Summary statistics for the 3-D geobody volumes across all of the model runs confirm what was noted previously: the mean values are highly skewed by the presence of a few large outliers, and the median values are often the smallest data value present (Table 4.7).

Table 4.7: Summary Statistics for 3-D Geobody Volume Distributions

3-D Geobody Volume Statistics

Input Sand%	Mean [m^3]	Median [m^3]	Std. Dev. [m^3]	Min. [m^3]	Max. [m^3]
20% Sand	9.68×10^3	125.00	1.30×10^6	125.00	1.91×10^8
30% Sand	1.43×10^4	125.00	1.87×10^6	125.00	2.56×10^8
40% Sand	4.55×10^4	125.00	3.95×10^6	125.00	3.46×10^8
50% Sand	1.22×10^5	125.00	7.33×10^6	125.00	4.45×10^8
60% Sand	3.65×10^5	125.00	1.40×10^7	125.00	5.37×10^8
70% Sand	1.64×10^6	125.00	3.16×10^7	125.00	6.12×10^8
Gradual	4.86×10^4	125.00	4.32×10^6	125.00	3.88×10^8
Abrupt	2.27×10^4	125.00	2.75×10^6	125.00	3.41×10^8

Chapter 5: Discussion

5.1 Hypothesis A

Hypothesis A posited the notion that process-based modeling produces stratigraphy that is different from randomly arranged stratigraphy. This is not a new hypothesis; stratigraphers and reservoir modelers have known for some time now that process-mimicking models produce stratigraphy with long-scale continuity and emergent features resembling real geology (Hoffimann, Scheidt, Barfod, & Caers, 2017; M. Pyrcz et al., 2014). Process-mimicking models are popular because true physics modeling is believed to be unfeasible at this time due to a lack of complete understanding of physical processes, and a lack of adequate computing power (Miller et al., 2008).

The synthetic stratigraphy generated provides alternative cases in which the process-based development of the stratigraphy is eroded, and the assemblage of the sand and mud parcels is more random. The autocorrelation analysis and results presented (Section 4.1.1), show the increase in the autocorrelation initial decay rate as the shuffling introduces more randomness to the system. These results hold true for the edge cases of the muddy (20% input sand) and the sandy (70% input sand) modeled systems.

5.2 Hypothesis B

Hypothesis B, broadly questions the potential linkage between surface channel features and mobility, and the sand features preserved in the stratigraphy. This relationship is examined using bulk delta parameters, and also more local measurements related to data collected from strike transects.

5.2.1 Hypothesis B(i)

Hypothesis B(i) suggested that channel depth would be a control on sand body thickness in the stratigraphy. To evaluate this relationship, the average channel depth along strike transects is compared to the average size of the vertical sand packages found in the strike section (Figure 5.1). Strike sections are taken at distances of 1, 1.5, and 2 km from the inlet.

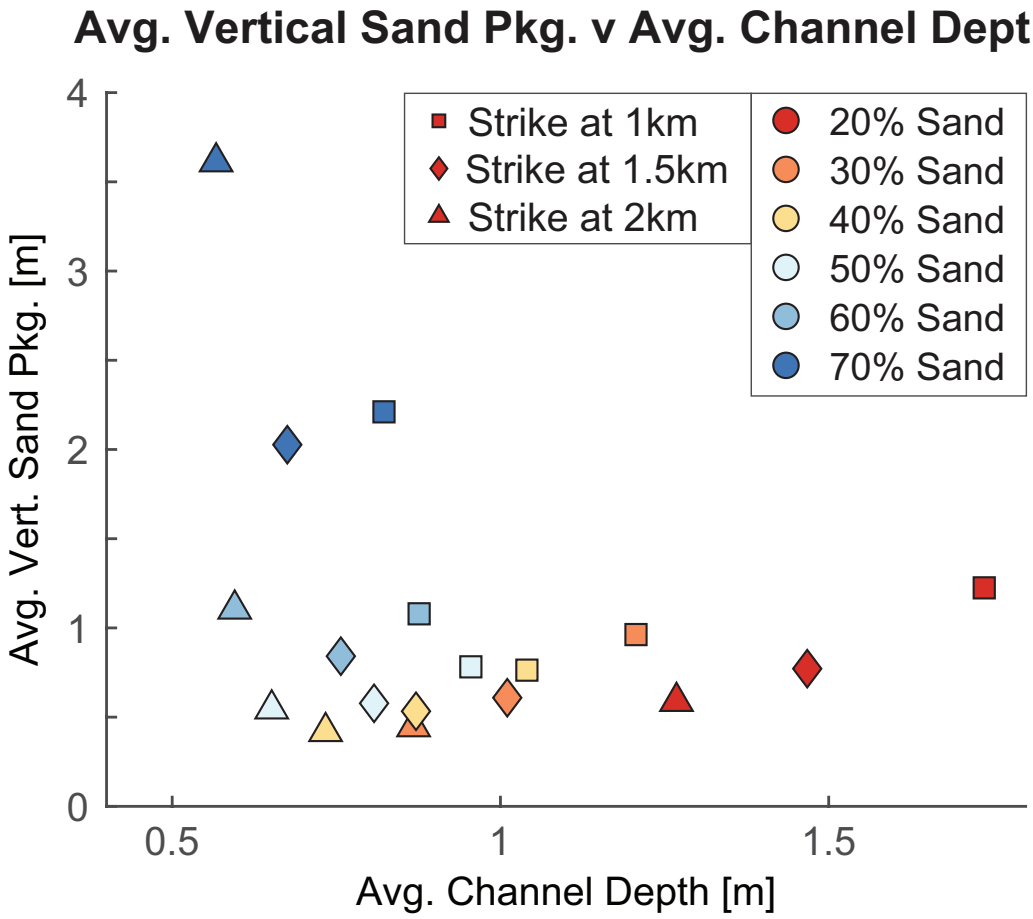

Figure 5.1: Average vertical sand packages in meters plotted against the average channel depth value recorded along the strike transect.

Decreasing channel depth and correspondingly thinner sand packages are observed in the 20, 30, 40, and 50% input sand scenarios, however this simple intuitive relationship is not entirely valid for the highly sandy (60 and 70% input sand) cases (Figure 5.1). In all input sand cases, the channel depths decrease as the distance from the inlet increases. Unlike the channel depth, the averaged vertical sand package size for the sandy cases does not always decrease as the distance from the inlet increases. We hypothesize that at high proportions (>50%), the sheer volume of sand in the system leads to columns that are mostly sand, and increases

this vertical sand package size as a result. When there is less mud present in the system, it is much easier to accumulate a large body of sand, and so although the surface channels are becoming more shallow, the subsurface sand features are being dominated by the bulk amount of sand input into the system. When 2-D geobodies are extracted from the strike section, similar behavior is observed. The channel depth along the strike transects is related to the ultimate areas of the geobodies identified from the strike stratigraphy (Figure 5.2). The scenarios with low (<50%) input sand proportions tend to follow the expected trend of decreasing channel depth and geobody area as distance from the inlet increases. However, just like vertical sand package sizes, the average geobody area increases once the input sand proportion is exceeds 50% (Figure 5.2).

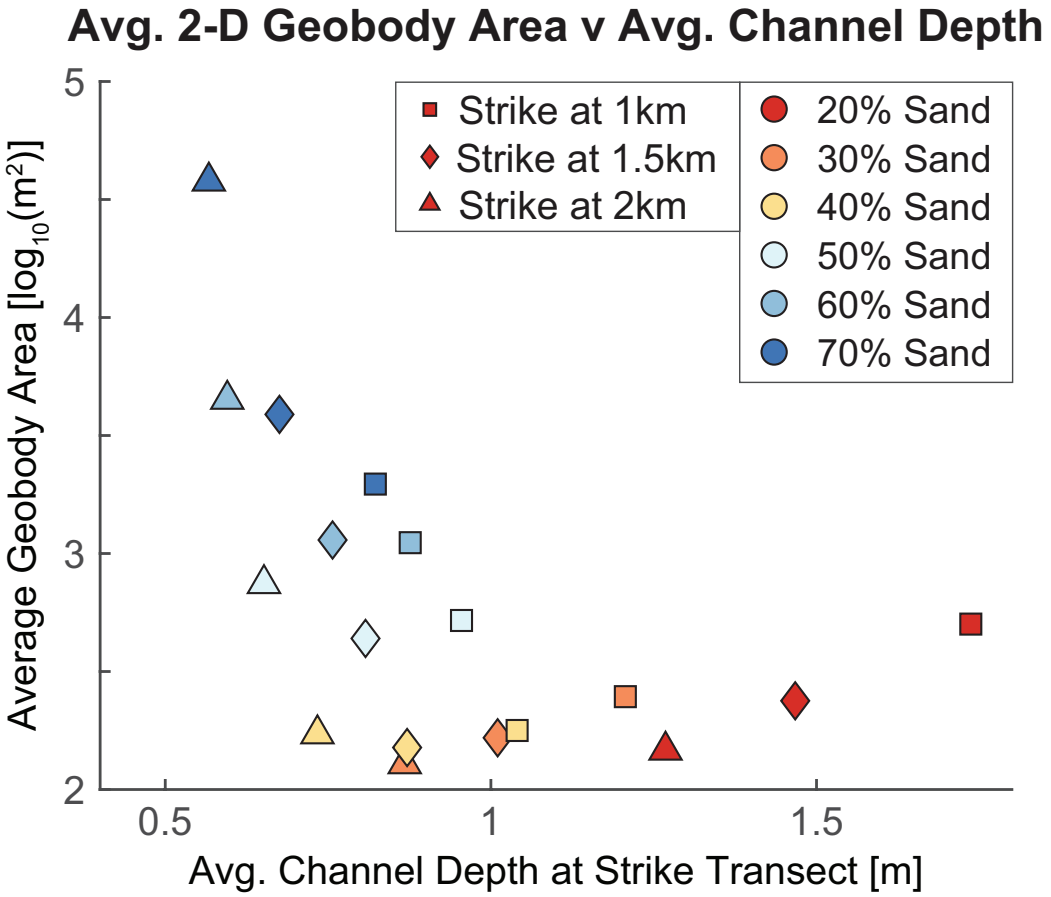

Figure 5.2: Average geobody area from strike section plotted against the average channel depth value recorded along the strike transect.

5.2.2 Hypothesis B(ii)

In Hypothesis B(ii), the channel mobility was expected to correlate with the size of the sand bodies preserved in the stratigraphy. Channel planform decay was taken as the measure of channel mobility in this work. Channel decay data was fit using an exponential decay function, from that fit, the parameter b represents the rate of the planform decay. The 3-D geobody volumes can be used as the reference values to represent the size of the sand bodies formed in the stratigraphy. The

relationship between channel decay and geobody volume is one method of relating surface processes to subsurface structure (Figure 5.3). The differences in planform decay rates between the different models is subtle, making this relationship not extremely informative, and ultimately inconclusive when relating surface channel mobility to preserved sand elements.

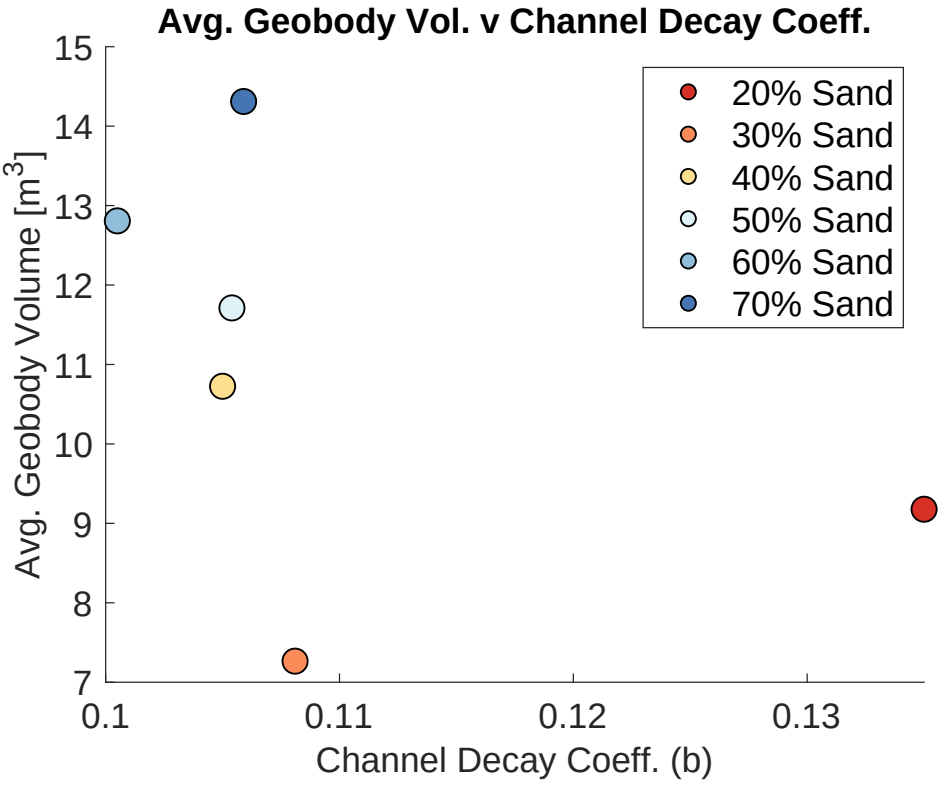

Figure 5.3: Average geobody volume plotted against the rate of channel planform decay.

The entrograms computed over the strike sections provide another way of examining the scales at which features are preserved in the subsurface. The range of the entrogram provides a length scale over which spatial continuity exists (similar to the variogram). There appears to be a loose relationship in which deeper channels have longer spatial correlation ranges (Figure 5.4). This finding agrees

with the notion that deeper channels leave deeper sand lenses in the stratigraphy, which is why we expected to see longer correlation lengths when the channels are deeper.

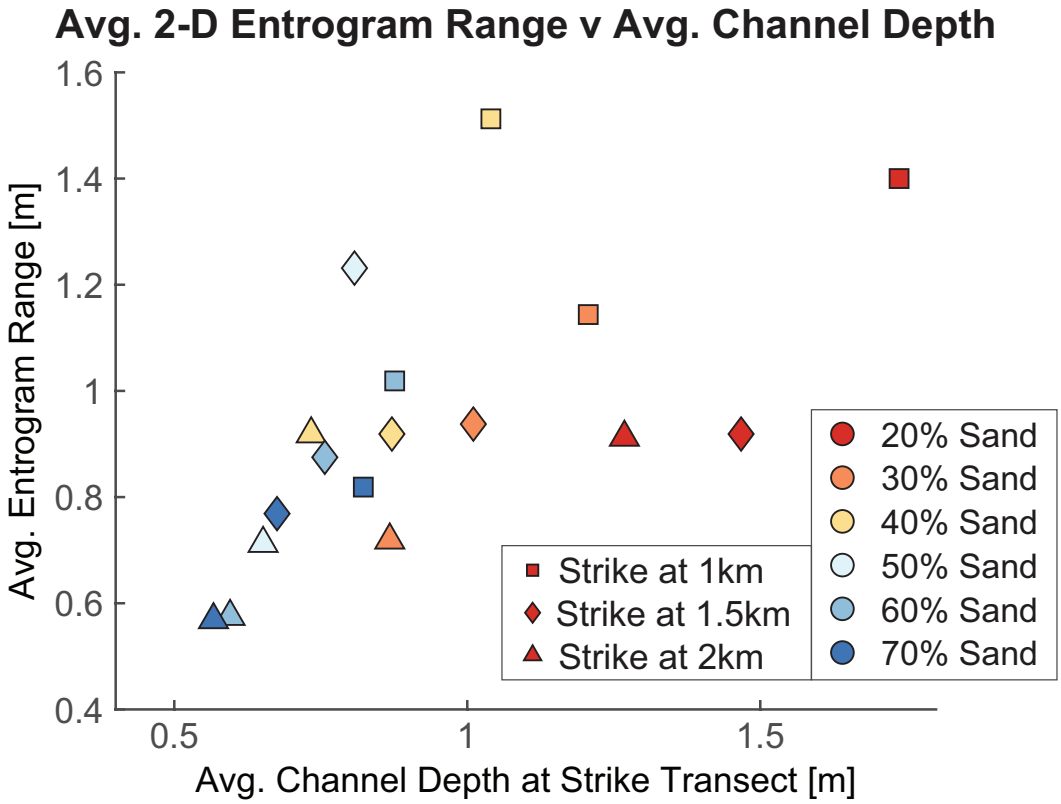

Figure 5.4: Average 2-D entrogram ranges are plotted against the corresponding average channel depths for the strike transects.

5.2.3 Hypothesis B(iii)

Hypothesis B(iii) expected to see correlation between channel properties on the delta surface and the preservation of features in the subsurface. To test this, the relationship between the average geobody volume for different scenarios is plotted against the average channel depth (Figure 5.5) and against the average channelized fraction for the delta (Figure 5.6). For both of these scenarios, a power-law

equation has been fit to the data. In both cases, the power-law fit appears to breakdown as the input sediment proportions become mud-dominated. We hypothesize that this deviation from the trend is related to the percolation threshold, which is known to be 31% for a random 3-D field (Hovadik & Larue, 2007). While the deltaic subsurface is certainly not a random field, a percolation threshold above which most, if not all of the sand in the system is linked may still exist. We hypothesize that above this percolation threshold, a massive geobody exists and overwhelmingly influences the mean geobody volume. Below the threshold, this skewing effect may still be present, but we expect it to be reduced as the bulk fraction of sand in the system is lesser.

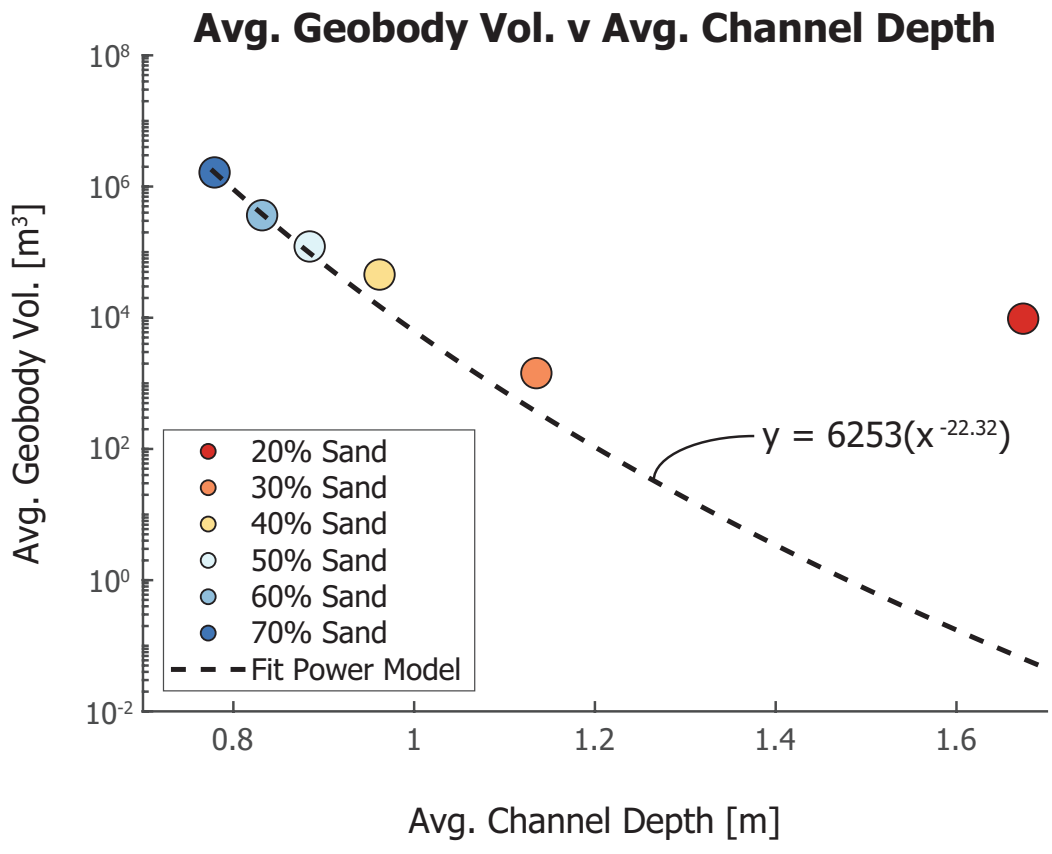

Figure 5.5: Average geobody volume plotted against the average channel depth.

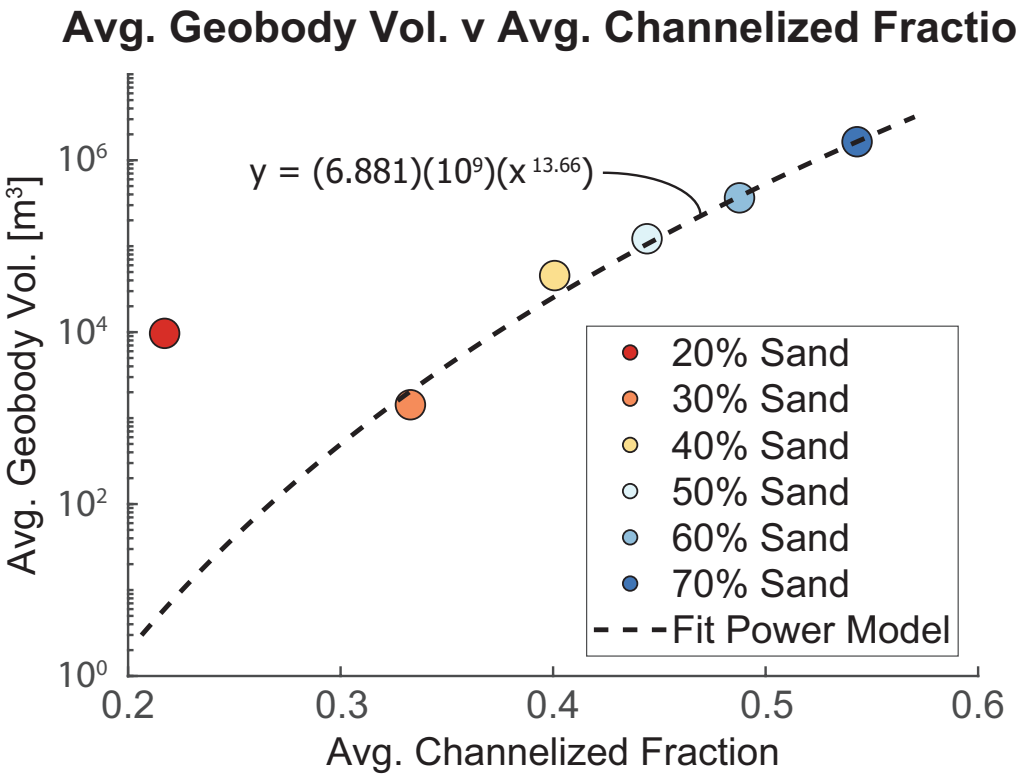

Figure 5.6: Average geobody volume plotted against the average channelized fraction.

5.3 Hypothesis C

Hypothesis C examines how a change in the composition of the inlet sediment manifests itself in the surface and ultimate subsurface structure for a river delta. The two scenarios modeled consisted of a gradual shift from a mud-dominated system with an input sand proportion of 20% to a sandy system with 70% of the input sediment being comprised of sand by the end of the simulation (Figure 3.4). The second scenario was one in which an abrupt shift from a muddy input to a sandy input is made; the simulation begins with a 20% input sand condition and shifts to 70% input sand abruptly after 480 years. For the gradually varying case,

the final proportion of sand is 45% and for the abrupt varying case it is 40% sand.

5.3.1 Varying Cases - Channel Properties

The bulk channel depth statistics for these variable input cases agree well with their corresponding steady input sand cases of 40% and 45% input sand respectively (Tables 4.2 & 4.3). But, in the abrupt scenario, the average channel depth before the shift in input sediment resembled the 20% sand steady input case, and the average channel depth after the shift was below the 60% sand input case, and approaching the value of the 70% input sand case. This channel depth behavior suggests, that the system would have re-equilibrated with channel depths distributed similar to the steady input 70% sand case if given more time. In the gradual varying case it is harder to draw conclusions from the channel depth data before and after the input sediment became majority sand. The average values before and after that transition do suggest however, that the channels became shallower on average as the input sand concentration grew higher.

However, when it comes to the overall channelized fraction, and the channel decay behavior, the variable input sand cases are closer to their initial condition of 20% input sand than they are to the final 70% input cases (Figures 4.8 & 4.10). The channelized fraction and channel decay metrics fall below the values found for the 30% sand steady input cases, suggesting that the topography and dynamics set up initially when the sand input is low, have lasting effects on the channel dynamics throughout the simulation.

5.3.2 Varying Cases - Subsurface Characterization

In the subsurface, the two scenarios behave quite differently. The gradual varying case has average sand packages larger than what would be expected from a steady 45% sand input scenario (Table 4.5). The abrupt case contains much larger average sand package values than would be expected for a steady 40% input sand case, the vertical sand package values more closely approach the 70% input sand case than any other. The gradually varying input sand case has descriptive statistics that fall between the steady 40% and 50% input sand results, which would be inline with a steady 45% input sand case (Table 4.7). The abruptly varying input case, on the other hand, has a mean value that is approximately half of what was obtained for the analogous 40% sand steady input scenario. This discrepancy suggests that the abrupt change in input sand results in a unique subsurface that greatly differs from its steady input analog.

The entrogram is a statistic that assumes stationarity; by varying the input fraction of sand to the system, the resulting strike sections are nonstationary in nature. So while the averaged spatial correlation scales (Table 4.6) are much higher in the variable input sand cases, those findings are likely artifacts of the highly nonstationary strike sections produced by varying the input sand conditions, not actual spatial continuity.

Chapter 6: Conclusions and Future Work

6.1 Conclusions

In conclusion, this work supports the notion that surface channel behavior influences the subsequent subsurface structure developed in a forward evolving process-based model such as DeltaRCM. Different input sediment proportions were used to generate different surface channel behaviors, and these channel properties were compared to the distribution and structure of the sand particles preserved in the stratigraphy.

By randomly re-ordering the modeled subsurface and comparing the autocorrelation of those fields to the modeled fields, the importance of the process-based modeling was confirmed. After affirming the translation of process-based modeling to significant subsurface structure, surface channel properties were compared to sand bodies preserved in the subsurface. While some subsurface properties were dominated by the bulk sediment proportions, the results suggest that larger sand bodies are present when there are many shallow channels versus few deep channels. However the spatial continuity of the field appears to increase when the channels are fewer in number and deeper. These findings are consistent with previous studies and support the proposed hypotheses. Varying the input sediment proportions over the course of the simulation produced unique results which did not match the findings for analogous steady input conditions.

6.2 Future Work

Moving forward, the DeltaRCM model will be used to simulate delta evolution under different relative sea level rise forcing conditions. By doing so, the influence of the sea level rise on the stratigraphy will be quantifiable. Other modeling scenarios will be considered such as an initial sloping basin, variable input discharges, and variable sea level rise scenarios.

This work has confirmed previous findings that the input conditions and surface behavior are linked to subsurface structure and expression (Liang, Kim, & Passalacqua, 2016). To move beyond correlation and to imply causation or a quantifiable linkage between surface behavior and subsurface form, future work will leverage tools from information theory to quantify causal links between surface dynamics and subsurface form. Long-term plans include the extension of DeltaRCM to incorporate tidal and wave forcings in an effort to model deltas from other sides of Galloway's triangle.

Appendices

A Model Parameters

Table A.1: Full Model Parameters

Extended List of Model Parameters

Parameter	*Value*
Simulation Duration	800 years
Cell Dimensions (X × Y × Z)	50m x 50m x 5cm
Initial Sea Level Elevation	0m
Relative Sea Level Rise	60 mm/year
Inlet Channel Width	250 m
Inlet Water Flux	1250 m^3/s
Inlet Sediment Flux	1.25 m^3/s
Basin Depth	5 m
Additional Parameters	*Value*
Inlet Channel Velocity	1.0m/s
Number of 'Parcels' (Water & Sediment)	2000
Sediment Deposition/Erosion Parameters	*Value*

Table A.2: Additional Model Parameters

Extended List of Model Parameters

Parameter	*Value*
Mud Deposition Velocity Threshold	0.3 m/s
Sand Erosion Velocity Threshold	1.05 m/s
Mud Erosion Velocity Threshold	1.5 m/s
Random Walk Parameters	*Value*
theta_water & theta_mud	1.0
theta_sand	2.0
Smoothing/Diffusion Parameters	*Value*
beta	3
lambda	1.0
alpha	0.1
Nsmooth	10
Csmooth	0.9

B 3-D Model Output Visualizations

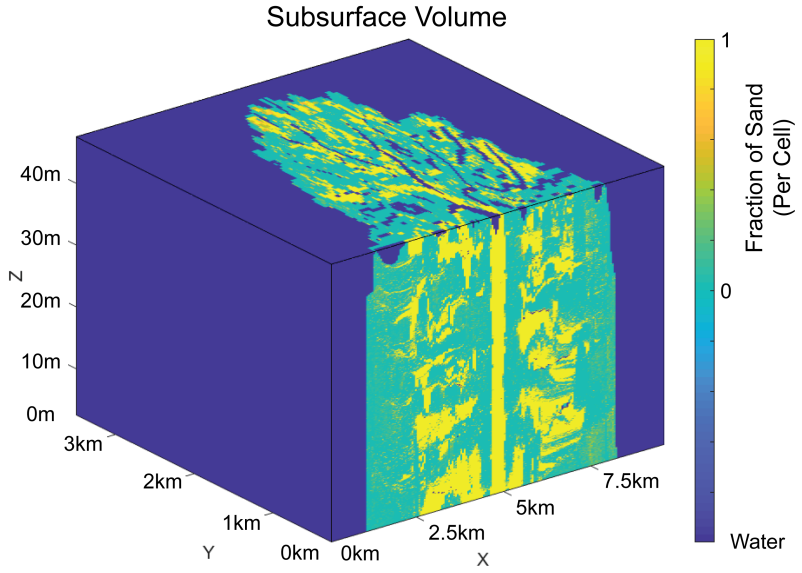

Figure B.1: 3-D visualization of a final subsurface output of a given model, including the surrounding water in the domain

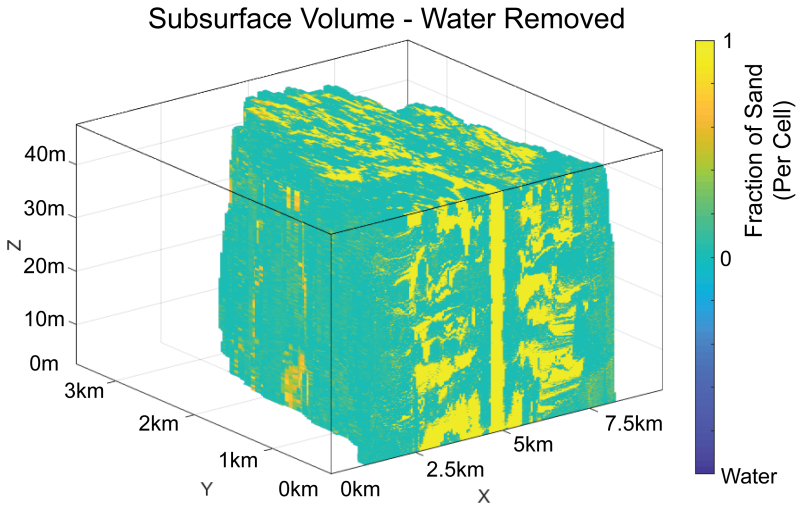

Figure B.2: 3-D visualization of a final subsurface output of a given model, without the surrounding water

C Additional Strike Sections

C.1 Strike Sections 1km from Inlet

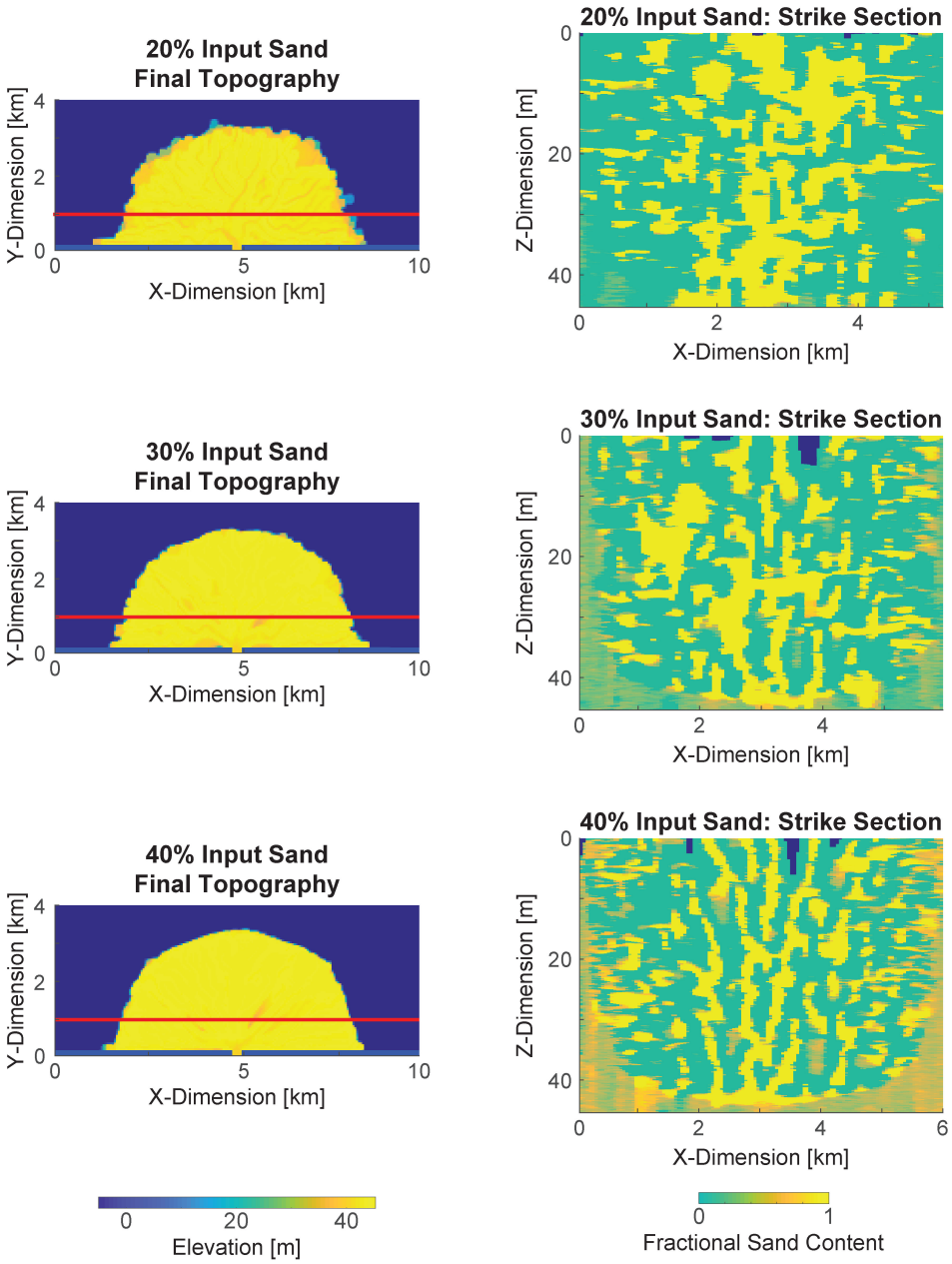

Figure C.3: Final model topographies with associated strike sections taken 1.0km from the inlet

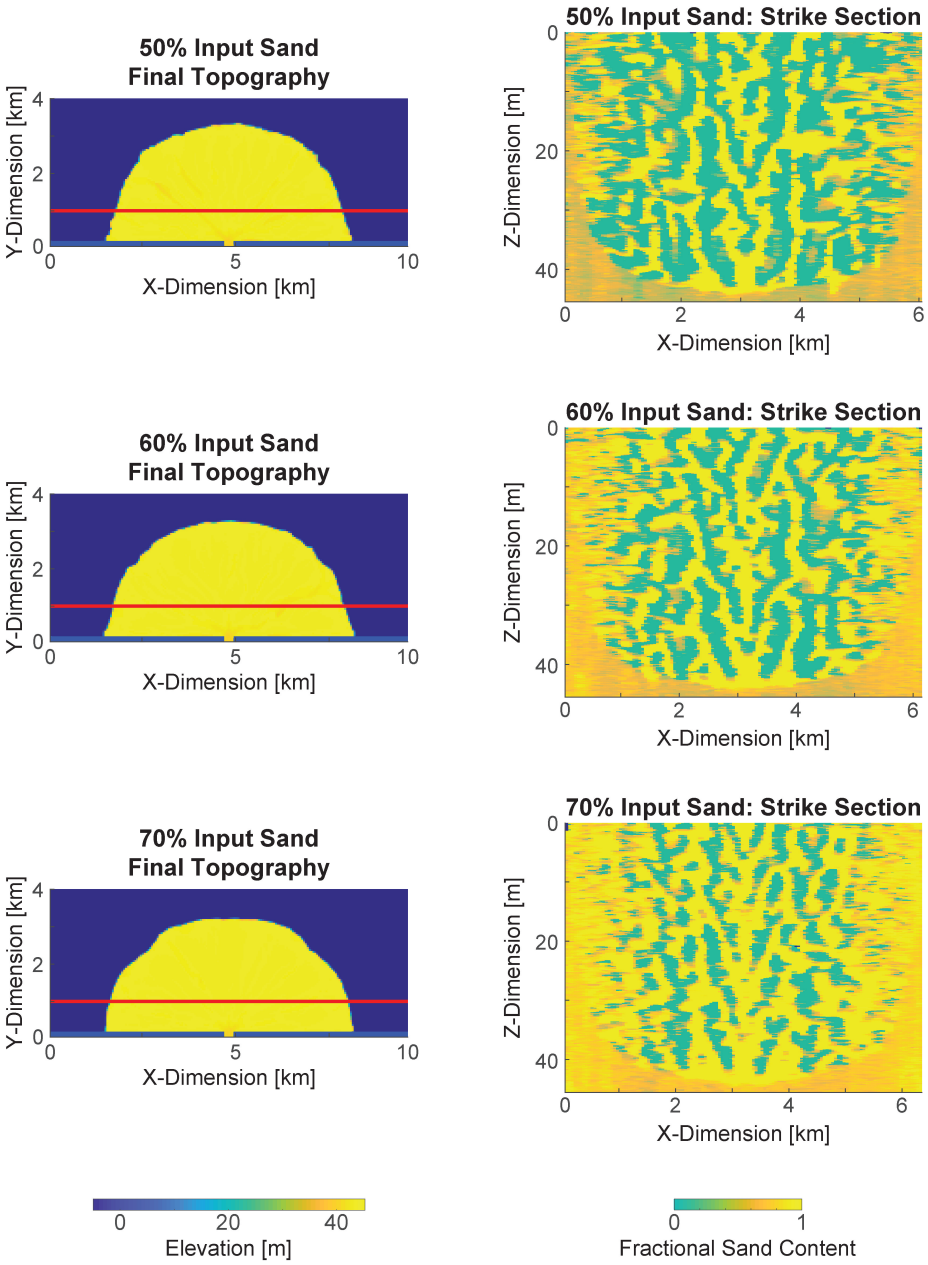

Figure C.4: Final model topographies with associated strike sections taken 1.0km from the inlet

C.2 Strike Sections 2km from Inlet

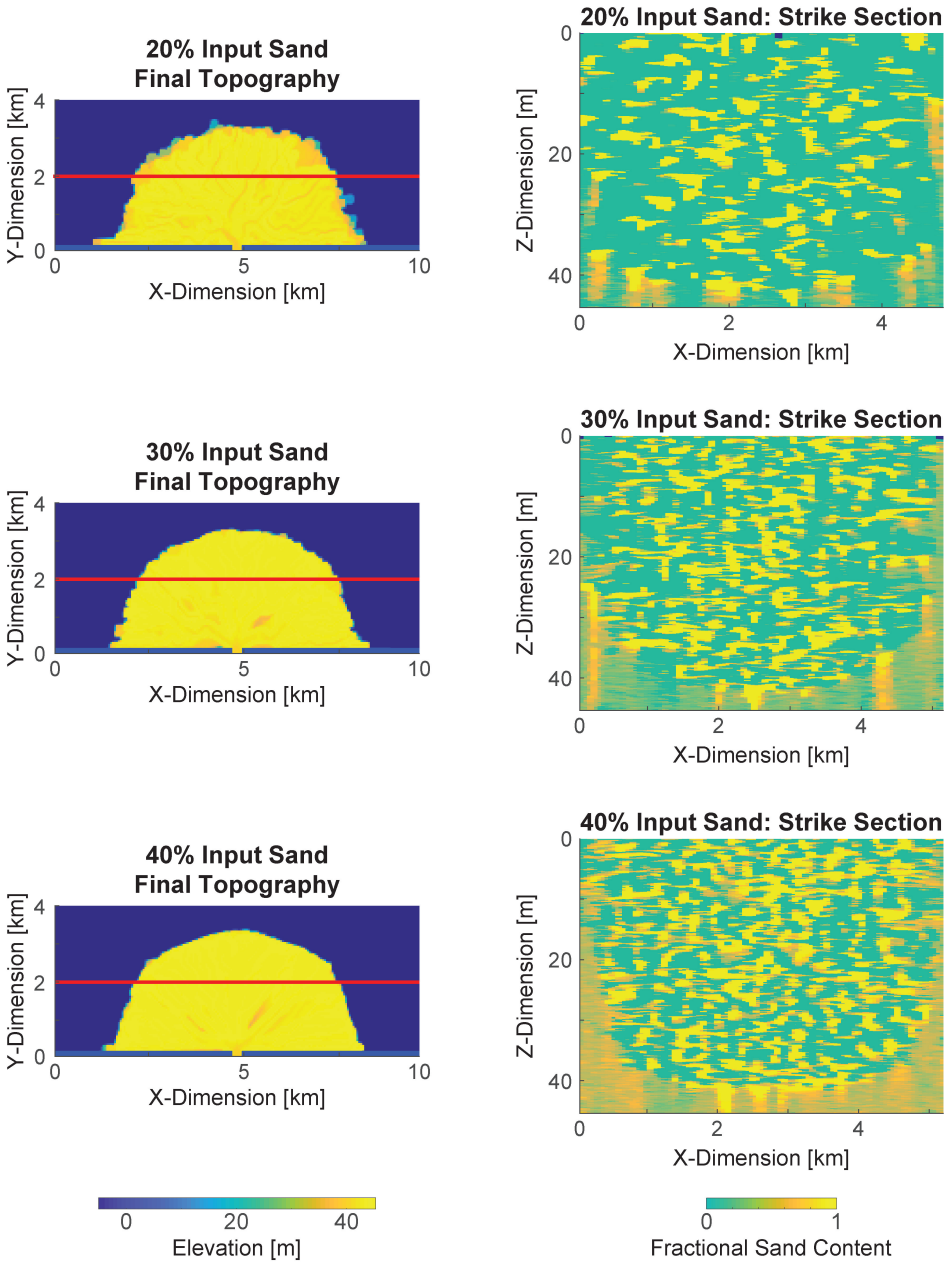

Figure C.5: Final model topographies with associated strike sections taken 2.0km from the inlet

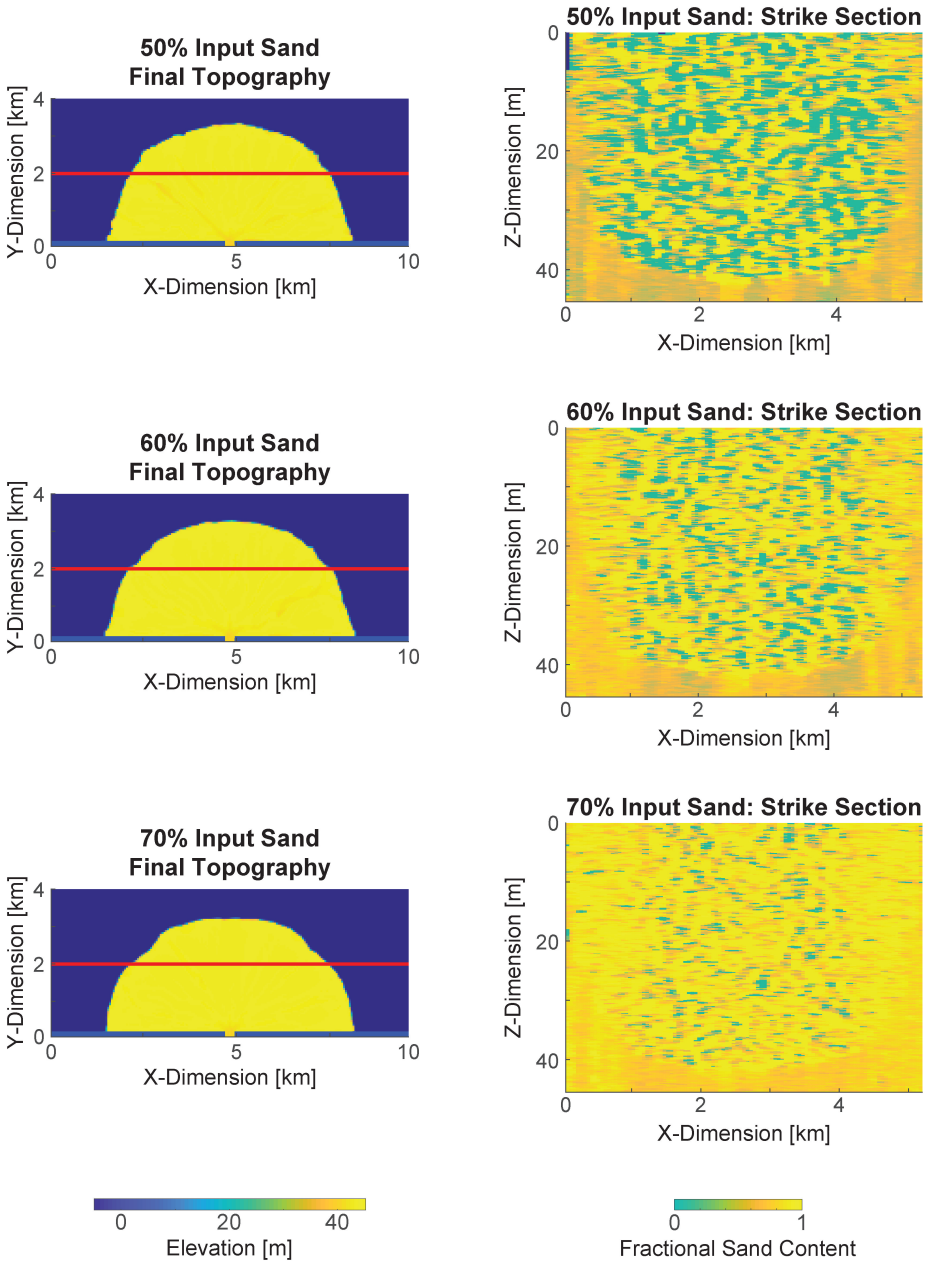

Figure C.6: Final model topographies with associated strike sections taken 2.0km from the inlet

D Dip Sections

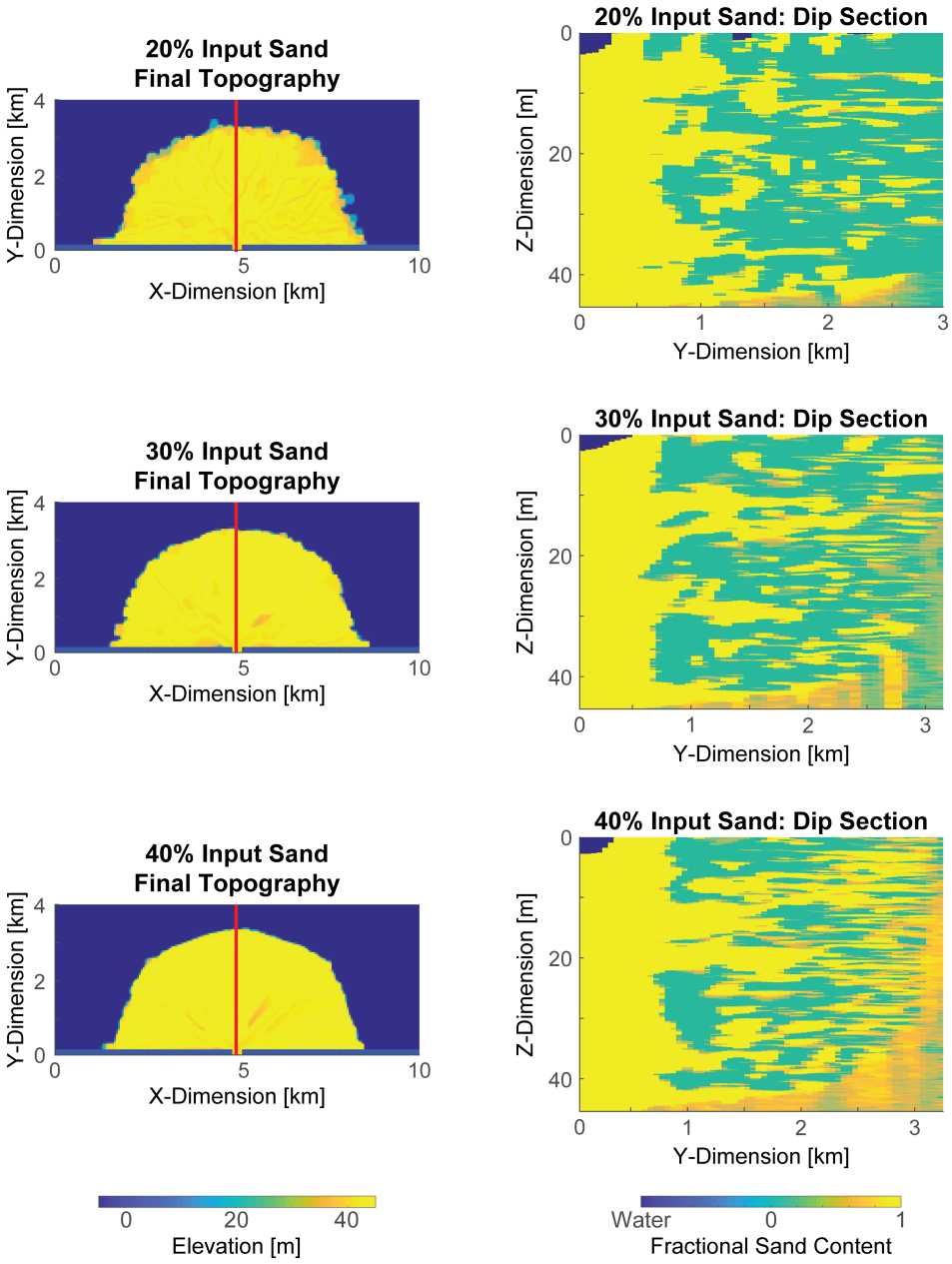

Figure D.7: Final model topographies with associated dip sections taken inline with the inlet mouth

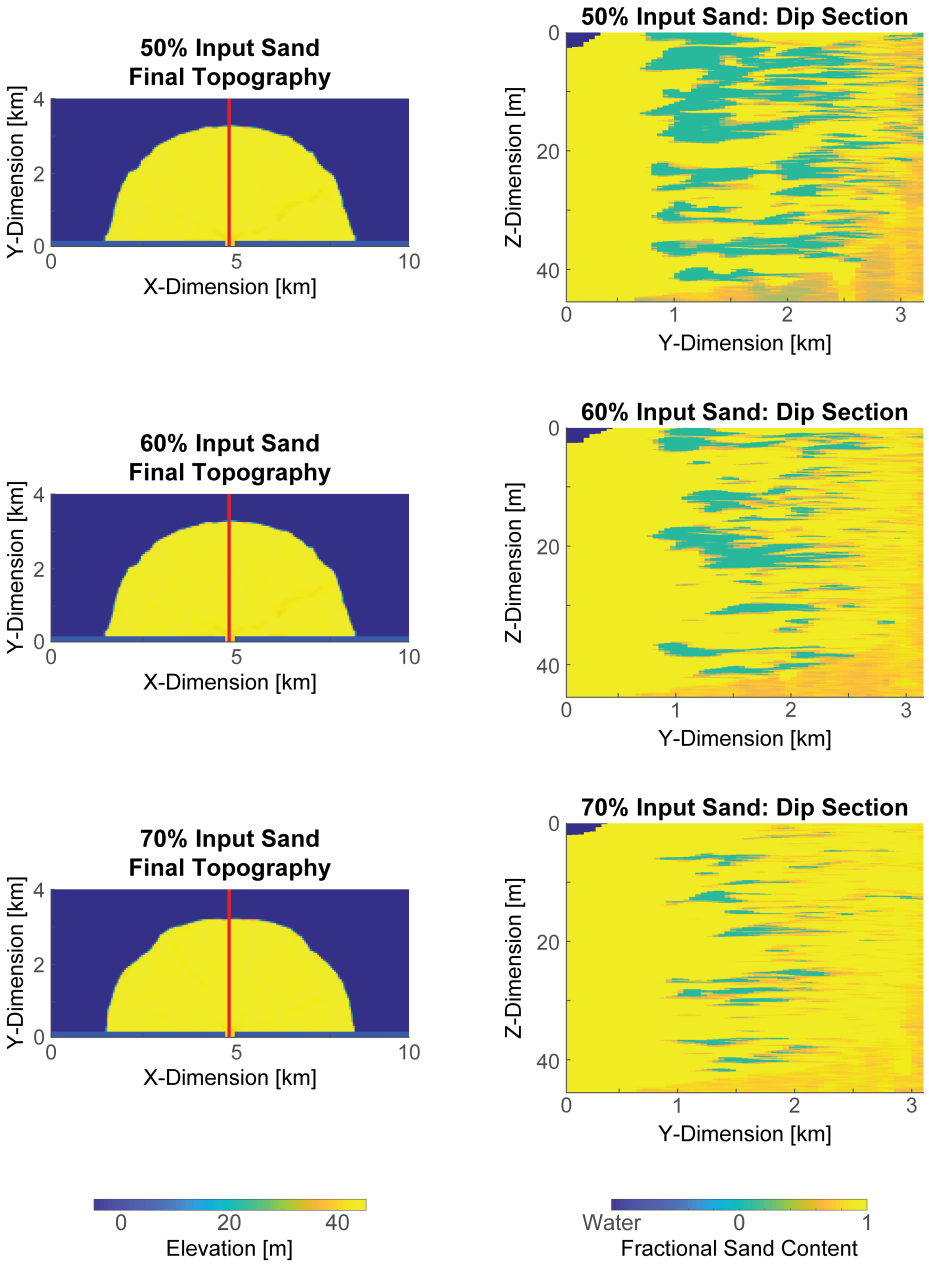

Figure D.8: Final model topographies with associated dip sections taken inline with the inlet mouth

E Shuffling Autocorrelation Results

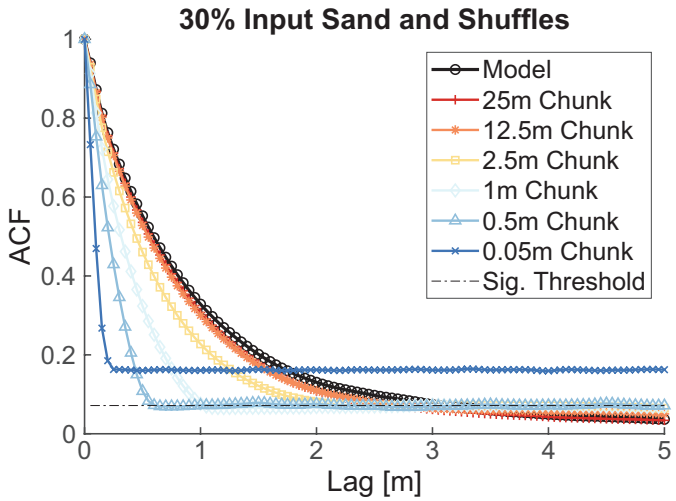

Figure E.9: Autocorrelation function for 30% input sand model and shuffled scenarios

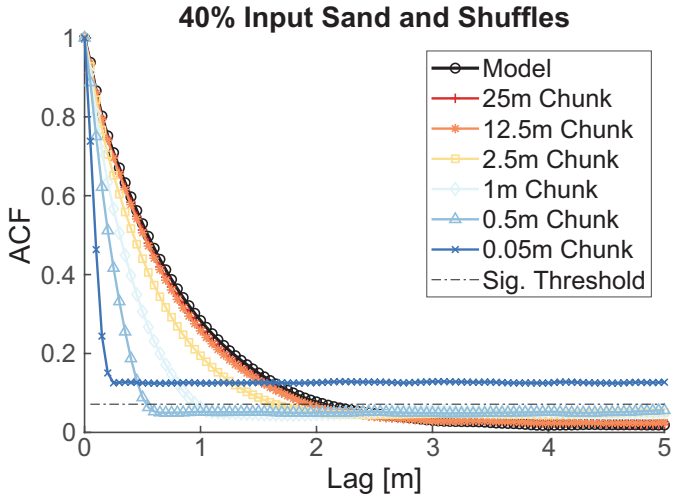

Figure E.10: Autocorrelation function for 40% input sand model and shuffled scenarios

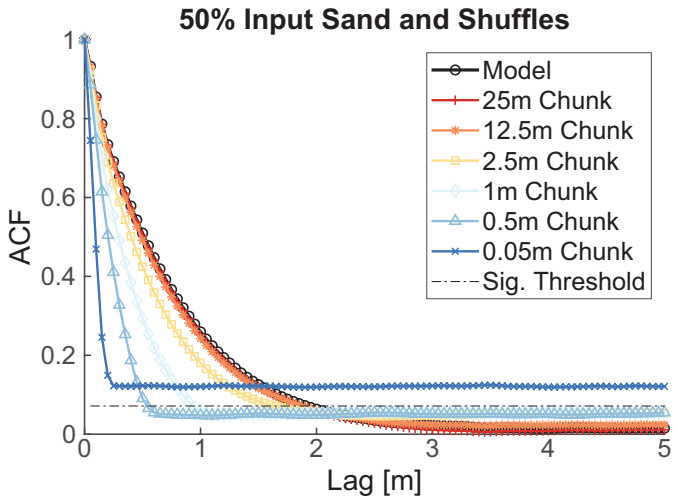

Figure E.11: Autocorrelation function for 50% input sand model and shuffled scenarios

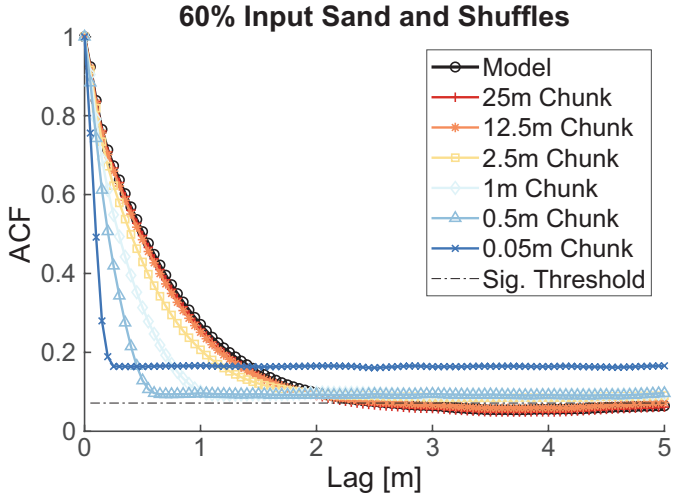

Figure E.12: Autocorrelation function for 60% input sand model and shuffled scenarios

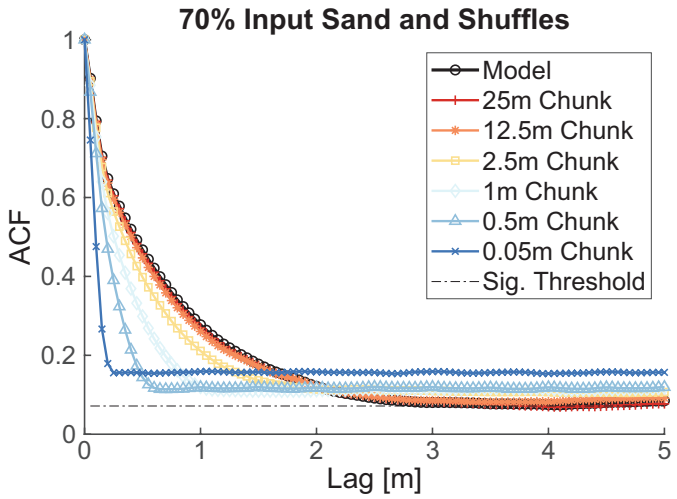

Figure E.13: Autocorrelation function for 70% input sand model and shuffled scenarios

References

Barrell, J. (1917, jan). Rhythms and the measurements of geologic time. *Geological Society of America Bulletin*, *28*(1), 745–904. Retrieved from https://pubs.geoscienceworld.org/gsabulletin/article/28/1/745-904/2867 doi: 10.1130/gsab-28-745

Bianchi, M., & Pedretti, D. (2018, jun). An entrogram-based approach to describe spatial heterogeneity with applications to solute transport in porous media. *Water Resources Research*. Retrieved from http://doi.wiley.com/10.1029/2018WR022827 doi: 10.1029/2018WR022827

Cazanacli, D., Paola, C., & Parker, G. (2002, mar). Experimental Steep, Braided Flow: Application to Flooding Risk on Fans. *Journal of Hydraulic Engineering*, *128*(3), 322–330. Retrieved from http://ascelibrary.org/doi/10.1061/{%}28ASCE{%}290733-9429{%}282002{%}29128{%}3A3{%}28322{%}29 doi: 10.1061/(ASCE)0733-9429(2002)128:3(322)

Deltares. (2016). *Delft3D 3D/2D modelling suite for integral water solutions User Manual.* Retrieved from https://content.oss.deltares.nl/delft3d/manuals/Delft3D-FLOW{_}User{_}Manual.pdfhttps://oss.deltares.nl/documents/637298/641496/D-Flow{_}FM{_}User{_}Manual

.pdf{%}0Ahttp://content.oss.deltares.nl/delft3d/manuals/Delft3D-FLOW{_}User{_}Manual.pdf

Dyk, C. J. V. (2015). *Validation of a reduced-complexity numerical model for resolving deltaic dynamics : internal consistency and morphodynamics APPROVED BY SUPERVISING COMMITTEE :* (Unpublished doctoral dissertation). University of Texas at Austin.

Galloway, W. E. (1975). Process framework for describing the morphological and stratigraphic evolution of deltaic depositional systems, in: M. L. Broussard, ed., Deltas, models for exploration. *Texas, Houston Geological Society*, 87–98. Retrieved from http://archives.datapages.com/data/hgssp/data/022/022001/87{_}hgs0220087.htm

Hoffimann, J., Scheidt, C., Barfod, A., & Caers, J. (2017, sep). Stochastic simulation by image quilting of process-based geological models. *Computers & Geosciences*, *106*, 18–32. Retrieved from https://www.sciencedirect.com/science/article/pii/S0098300417301139 doi: 10.1016/J.CAGEO.2017.05.012

Hovadik, J. M., & Larue, D. K. (2007, aug). Static characterizations of reservoirs: refining the concepts of connectivity and continuity. *Petroleum Geoscience*, *13*(3), 195–211. Retrieved from http://pg.lyellcollection.org/cgi/doi/10.1144/1354-079305-697 doi: 10.1144/1354-079305-697

Isikdogan, F., Bovik, A., & Passalacqua, P. (2017, dec). RivaMap: An automated river analysis and mapping engine. *Remote Sensing of Environment*, *202*, 88–97. Retrieved from https://www.sciencedirect.com/science/article/pii/S0034425717301475 doi: 10.1016/j.rse.2017.03.044

Jerolmack, D. J., & Paola, C. (2010, oct). Shredding of environmental sig-

nals by sediment transport. *Geophysical Research Letters*, *37*(19). Retrieved from http://doi.wiley.com/10.1029/2010GL044638 doi: 10.1029/2010GL044638

Jørgensen, F., Høyer, A. S., Sandersen, P. B., He, X., & Foged, N. (2015, aug). Combining 3D geological modelling techniques to address variations in geology, data type and density - An example from Southern Denmark. *Computers and Geosciences*, *81*, 53–63. Retrieved from https://www.sciencedirect.com/science/article/pii/S009830041500093X?via{%}3Dihub doi: 10.1016/j.cageo.2015.04.010

Khan, M. R., Koneshloo, M., Knappett, P. S. K., Ahmed, K. M., Bostick, B. C., Mailloux, B. J., ... Michael, H. A. (2016). Megacity pumping and preferential flow threaten groundwater quality. *Nature Communications*, *7*. Retrieved from https://search-proquest-com.ezproxy.lib.utexas.edu/docview/1823511985?pq-origsite=summon doi: 10.1038/ncomms12833

Kim, W., Mohrig, D., Twilley, R., Paola, C., & Parker, G. (2009, oct). Is It Feasible to Build New Land in the Mississippi River Delta? *Eos, Transactions American Geophysical Union*, *90*(42), 373–374. Retrieved from http://doi.wiley.com/10.1029/2009EO420001 doi: 10.1029/2009EO420001

Liang, M., Geleynse, N., Edmonds, D. A., & Passalacqua, P. (2015). A reduced-complexity model for river delta formation – Part 2: Assessment of the flow routing scheme. *Earth Surf. Dynam*, *3*, 87–104. Retrieved from www.earth-surf-dynam.net/3/87/2015/ doi: 10.5194/esurf-3-87-2015

Liang, M., Kim, W., & Passalacqua, P. (2016, oct). How much subsidence is enough to change the morphology of river deltas? *Geophysical Research Letters*, *43*(19), 10,266–10,276. Retrieved from http://doi.wiley.com/

10.1002/2016GL070519 doi: 10.1002/2016GL070519

Liang, M., Van Dyk, C., & Passalacqua, P. (2016, feb). Quantifying the patterns and dynamics of river deltas under conditions of steady forcing and relative sea level rise. *Journal of Geophysical Research: Earth Surface*, *121*(2), 465–496. Retrieved from http://doi.wiley.com/10.1002/2015JF003653 doi: 10.1002/2015JF003653

Liang, M., Voller, V. R., & Paola, C. (2015). A reduced-complexity model for river delta formation – Part 1: Modeling deltas with channel dynamics. *Earth Surf. Dynam*, *3*, 67–86. Retrieved from www.earth-surf-dynam.net/3/67/2015/ doi: 10.5194/esurf-3-67-2015

Linde, N., Renard, P., Mukerji, T., & Caers, J. (2015, dec). Geological realism in hydrogeological and geophysical inverse modeling: A review. *Advances in Water Resources*, *86*, 86–101. Retrieved from https://www.sciencedirect.com/science/article/pii/S0309170815002262?via{%}3Dihub doi: 10.1016/J.ADVWATRES.2015.09.019

Matheron, G. (1963, dec). Principles of geostatistics. *Economic Geology*, *58*(8), 1246–1266. Retrieved from http://pubs.geoscienceworld.org/economicgeology/article/58/8/1246/17275/Principles-of-geostatistics doi: 10.2113/gsecongeo.58.8.1246

Miller, J., Sun, T., Li, H., Stewart, J., Genty, C., Li, D., & Lyttle, C. (2008). Direct Modeling of Reservoirs Through Forward Process-Based Models: Can We Get There? *Proceedings of International Petroleum Technology Conference*, 12729. Retrieved from http://www.onepetro.org/mslib/servlet/onepetropreview?id=IPTC-12729-MS{&}soc=IPTC doi: 10.2523/12729-MS

Moser, S. C., Jeffress Williams, S., & Boesch, D. F. (2012). Wicked Challenges at Land's End: Managing Coastal Vulnerability Under Climate Change. *Annual Review of Environment and Resources*, *37*(1), 51–78. Retrieved from http://www.annualreviews.org/doi/10.1146/annurev-environ-021611-135158 doi: 10.1146/annurev-environ-021611-135158

Olea, R. A. (2009). *A Practical Primer on Geostatistics. USGS*. Reston. Retrieved from https://pubs.usgs.gov/of/2009/1103/

Overeem, I., Syvitski, J. P., & Hutton, E. W. (2005). Three-Dimensional Numerical Modeling of Deltas. Retrieved from http://archives.datapages.com/data/sepm{_}sp/SP83/Three-Dimensional{_}Numerical{_}Modeling{_}of{_}Deltas.htm

Pyrcz, M., Sech, R., Covault, J., Sun, T., Willis, B., & Sylvester, Z. (2014). Process-mimicking Modeling Considerations. *Closing the gap II: advances in applied geomodelling for hydrocarbon reservoirs*, 1–16.

Pyrcz, M. J., Gringarten, E., Frykman, P., & Deutsch, C. V. (2006). Representative input parameters for geostatistical simulation. In *Stochastic modeling and geo- statistics: Principles, methods, and case studies, volume ii: Aapg computer applications in geology* (pp. 123–137). AAPG Special Volumes. Retrieved from http://archives.datapages.com/data/specpubs/ca05/CHAPTER10/CHAPTER10.HTMpapers2://publication/uuid/39F24F4E-A9C4-4140-8E63-C02138631364 doi: 10.1306/1063811CA53230

Rahman, M. M., Penny, G., Mondal, M. S., Zaman, M. H., Kryston, A., Salehin, M., ... Müller, M. F. (2019, mar). *Salinization in large river deltas: Drivers, impacts and socio-hydrological feedbacks* (Vol. 6). Retrieved from https://

linkinghub.elsevier.com/retrieve/pii/S2468312418300087 doi: 10.1016/j.wasec.2019.100024

Sadler, P. M., & Strauss, D. J. (1990, may). Estimation of completeness of stratigraphical sections using empirical data and theoretical models. *Journal of the Geological Society*, *147*(3), 471–485. Retrieved from http://jgs.lyellcollection.org/lookup/doi/10.1144/gsjgs.147.3.0471 doi: 10.1144/gsjgs.147.3.0471

Schwenk, J., Khandelwal, A., Fratkin, M., Kumar, V., & Foufoula-Georgiou, E. (2017, feb). High spatiotemporal resolution of river planform dynamics from landsat: The rivMAP toolbox and results from the Ucayali river. *Earth and Space Science*, *4*(2), 46–75. Retrieved from http://doi.wiley.com/10.1002/2016EA000196 doi: 10.1002/2016EA000196

Seybold, H., Andrade, J. S., & Herrmann, H. J. (2007, oct). Modeling river delta formation. *Proceedings of the National Academy of Sciences of the United States of America*, *104*(43), 16804–9. Retrieved from http://www.ncbi.nlm.nih.gov/pubmed/17940031http://www.pubmedcentral.nih.gov/articlerender.fcgi?artid=PMC2040410 doi: 10.1073/pnas.0705265104

Syvitski, J. P., Kettner, A. J., Overeem, I., Hutton, E. W., Hannon, M. T., Brakenridge, G. R., ... Nicholls, R. J. (2009, oct). Sinking deltas due to human activities. *Nature Geoscience*, *2*(10), 681–686. Retrieved from http://www.nature.com/articles/ngeo629 doi: 10.1038/ngeo629

The Mathworks Inc. (2018). *Image Processing Toolbox.* Natick, MA: Mathworks. Retrieved from https://www.mathworks.com/help/images/index.html

Trampush, S. M., Hajek, E. A., Straub, K. M., & Chamberlin, E. P. (2017).

Identifying autogenic sedimentation in fluvial-deltaic stratigraphy: Evaluating the effect of outcrop-quality data on the compensation statistic. *Journal of Geophysical Research: Earth Surface*, *122*(1), 91–113. doi: 10.1002/2016JF004067

Wheeler, H. E. (1958). Time-Stratigraphy. *AAPG Bulletin*, *42*(5), 1047–1063. Retrieved from `http://archives.datapages.com/data/bulletns/1957-60/data/pg/0042/0005/1000/1047.htm?doi=10.1306{%}2F0BDA5AF2-16BD-11D7-8645000102C1865D`

Wheeler, H. E. (1964, jul). Baselevel, lithosphere surface, and time-stratigraphy. *Geological Society of America Bulletin*, *75*(7), 599–610. Retrieved from `https://pubs.geoscienceworld.org/gsa/gsabulletin/article/75/7/599/5772/baselevel-lithosphere-surface-and-time` doi: 10.1130/0016-7606(1964)75[599:blsat]2.0.co;2

Wickert, A. D., Martin, J. M., Tal, M., Kim, W., Sheets, B., & Paola, C. (2013, apr). River channel lateral mobility: metrics, time scales, and controls. *Journal of Geophysical Research: Earth Surface*, *118*(2), 396–412. Retrieved from `https://doi.org/10.1029/2012JF002386` doi: 10.1029/2012JF002386